A critical assessment of design tools for stress analysis of adhesively bonded double lap joints

A Critical Assessment of Design Tools for Stress Analysis of Adhesively Bonded Double Lap Joints

Scott E Stapleton[a*], Bertram Stier[b], Stephen Jones[b], Andrew Bergan[c], Ibrahim Kaleel[d], Marco Petrolo[d], Erasmo Carrera[d], Brett A. Bednarcyk[e]

[a]*University of Massachusetts Lowell, Lowell, MA, 01854, U.S.A.*
[b]*Collier Research Corporation, Newport News, VA 23606, U.S.A.*
[c]*NASA Langley Research Center, Hampton, VA, 23666, U.S.A.*
Politecnico di Torino, Torino, 10129, Italy.
[e]*NASA Glenn Research Center, Cleveland, OH 44135, U.S.A.*

A Critical Assessment of Design Tools for Stress Analysis of Adhesively Bonded Double Lap Joints

Despite the proliferation of high fidelity finite element (FE) models, lower fidelity models remain commonly used in adhesively bonded joint design. These design models can save both computational and user time due to their simplicity and ease of use. In this study, a detailed assessment of local stress fields predicted by five design models: A4EI, HyperSizer, Joint Element Designer, Carrera Unified Formulation, and a Continuum Solid Shell FE model. All models were compared with a high fidelity, dense mesh FE model. Six double lap joint cases with different combinations of features like different adhereds, a core, and tapers.

Keywords: Adhesively Bonded Joints, Design, Modeling, Finite Element Analysis, Composite Materials, Sandwich, Honeycomb Core

1. Introduction

With the increasing demand for fiber reinforced composites in lightweight structures, adhesively bonded joints are becoming more prevalent than ever. Bolts and rivets require holes, which cut fibers and cause significant stress concentrations and can cause premature failure in composite materials. Adhesives spread the load more evenly over the composite while facilitating a lighter overall structure. Reductions in part count and touch labor can also result in significant cost reductions for adhesively bonded joints. The structural adhesive market in Europe has been forecasted to reach 67,000 tons by 2015, a growth of over 13 % since 2008.[1]

Analytical models for stress analysis have long been a part of initial adhesive joint design, analysis, and sizing. Despite the rise of general finite element software and methods, analytical design models remain a preferred method for fast and simple joint analysis due to stress singularities that are typical in bonded joints near reentrant corners. These models are constructed on the foundation of kinematic, geometrical, and material simplifications, along with assumptions that allow closed form or semi-closed form solutions. While the results are often relatively accurate, the primary value provided by these rapid tools is the ability to conduct sensitivity studies and assess criticality of various bonded joint geometries quickly. Because they typically require much less expertise and time commitment to generate high-quality results when compared to higher-fidelity methods, these tools fill a gap in the toolset of many stress engineers and designers.

This study compares and contrasts three semi-analytical methods and two relatively efficient finite element models. The semi-analytical methods are: (1) the A4EI code based on the methods of Hart-Smith[2,3], (2) the HyperSizer joints analysis capability based on extensions of the methods of Mortensen and Thomsen[4], and (3) the joint element designer (JED) based on the methods of Stapleton and co-workers[5]. The two efficient finite element models are: (4) a one-dimensional finite element model based on Carrera Unified Formulation (CUF), a variable kinematic higher-order 1D models that can produce high-fidelity solutions[6], and (2) a parametric continuum solid shell finite element model[7]. The results from these methods are compared with high-fidelity 3-D finite element results to show the implications of the assumptions used in each method for several exemplar bonded joint configurations. The joint configurations considered are: (1) double lap joint with aluminum adherends, (2) double lap joint with composite adherends, (3) stepped double lap joint with composite adherends, (4) double lap joint with composite adherends containing a honeycomb core, and (5) stepped double lap joint with composite adherends containing a honeycomb core.

2. Joint Configuration

Different joint configurations were analyzed in order to compare the joint analysis tools. The analyzed joint configurations, discussed in this section, range from simple to increasingly complex to pinpoint differences in the results from the various methods compared with the benchmark high-fidelity finite element results. In

this section, the material properties, geometries, and boundary conditions employed for the bonded joint cases are presented.

A. Materials

Material properties for the composite system and adhesive were obtained from open literature when possible. If data was not readily available for certain properties, notional values were assumed. Because this study sought to compare the behavior of several tools for identical problems rather than determine their absolute accuracy, notional values are acceptable. Table 1 through Table 5 provide the material properties for all material systems used in this study. All properties are the average of tension and compression unless otherwise noted.

B. Geometries and Boundary Conditions

As stated previously, the cases were conceived to progressively include increasing complexity to compare different features of the models. The final geometry (Cases 5 and 6) resembles a joint of interest for lauch vehicle primary structure, and the other examples were created by dropping one feature. The geometries are shown in Figure 1 and the corresponding boundary conditions are shown in Figure 2. Due to symmetry of the geometry and loading, only one half of each joint was modeled with symmetry boundary conditions in the middle.

Figure 1 here

Case 1 is a double lap joint with aluminum adherends under compression with the adherend restricted from rotation and vertical displacement at the point of loading. Case 2 has layered composite materials as the adherends, with the layups and materials noted in the Figure 1. The adherend was made by putting the two facesheets from the sandwich cases (Cases 4-6) together in one layup. Case 3 is a replica of Case 2 except that the doublers are stepped, dropping one ply per step. Case 4 is like Case 2 except with a core, the load split between two facesheets, and only the lower facesheet is restricted from vertical displacement at the point of loading. Finally, Cases 5 and 6 are the same geometry as Case 4 except with stepped doublers, and Case 6 is in a 3-pt bending configuration rather than axial compression.

Looking at the cases, Case 1 is the simplest, Case 2 adds composite adherends, Case 3 adds a taper, Case 4 adds a core with no taper, Case 5 adds a taper and core, and 6 adds load case complexity. In this way, differences in models can be isolated to specific features of the joints, one feature at a time.

Figure 2 here

C. Simplifying Assumptions

Although a total of six cases are studied in this work, several design features typical of double lap/double strap joints used in practice are not considered. First, the gap between the adherends (right side in Figure 1) is treated as a void herein whereas it is common to use a polymer filler material for manufacturability, which may affect the local stress distribution and the failure process. A second simplification is that the adhesive layer is treated with a linear elastic constitutive behavior when it is known that plastic deformation and fracture may occur. To be consistent with assuming a linear behavior in the adhesive, the applied loads are relatively low such that no significant plastic deformation or other nonlinearities are expected. It should be noted that all methods considered herein are capable of including nonlinear adhesive behavior. Another simplifying assumption is that an explicit adhesive layer is included in all cases; in some instances, a co-cured design is used where the doubler resin adheres the doubler to the adherend and no separate adhesive layer is used. A fourth simplifying assumption is that the doubler drop-off sequence is held at a constant taper angle with the same ply drop sequence for all cases such that the stresses due the ply drops are relatively low. In some designs, the doubler ply drop region may introduce much higher stress and therefore be more critical[12]. Lastly, it should be recognized that in practical structures, joints experience combined load conditions. Therefore, this paper represents a study of only elastic stress fields predicted by several rapid analysis tools in response to relatively simple loading conditions. It is of great interest to extend and apply rapid joint analysis tools to address several of the practical joint design features that have been omitted from this study.

3. Models

A. A4EI

A4EI is software developed based on the methods of Hart-Smith[2,13], which consider a 1-D semi-closed form solution for bonded joints. The adherends, which may be stepped, are modeled as truss members (with no bending) with homogenized section stiffnesses as input. The adhesive is treated as a bed of shear springs that can have an elastic-perfectly plastic shear response. The formulation involves application of equilibrium conditions to arrive at closed-form expressions for the axial deformation along the adherends. Integration constants appearing in these expressions, however, are determined via an iterative approach that can have convergence difficulties[2]. The A4EI solution provides the adhesive shear stresses and strains, as well as an average axial stress in the adherends, along the bonded joint. Given corresponding strength values as input, these can then be used to determine the strength of the joint. Notably, many versions of the code (including that used herein) do not include the adhesive peel stress in the formulation, although Hart-Smith does provide a simple solution for the approximate peak peel stress at the end of the joint[3]. Additionally, no ply-level stresses are calculated in the case of composite adherends. This limits A4EI's ability to predict delamination in the adherends, which is a common failure mode in composite bonded joints. Nevertheless, while the software dates from the 1970's, it is still used and can provide a reasonable estimate of adhesive shear stresses that can be used to size a joint given adhesive allowables.

B. HyperSizer

The bonded composite joint analysis capability within the HyperSizer structural sizing software[14] is based on Mortensen and Thompsen's[4] unified approach with extensions to compute ply level in-plane and interlaminar stresses, application of pressure loading, determine margins of safety based on a wide array of bonded joint specific failure criteria, and evaluate bond-line cracks with the Virtual Crack Closure Technique, see refs[15–17] for details. The joint adherends are treated as plates in generalized cylindrical bending, which allows for application uniform strain and uniform curvature in the direction normal to the joint analysis plane (i.e., the y-direction in Figure 1). The adherends are arbitrary composite laminates governed by classical lamination theory. The adhesive is treated as a continuously distributed layer of normal and shear springs whose constitutive response may be nonlinear. Boundary conditions are applied in the form of displacements/rotations or force/moment resultants.

The joint is divided into regions whose governing linear first-order differential equations are developed based on direct application of equilibrium. These equations are solved via the multi-segment method of integration presented by Mortensen and Thompsen[4]. The joint regions are each divided into small segments, and the solution of each segment is determined using direct integration. Continuity between these segments and between the joint regions is enforced, while accounting for any midplane shifts because of changes in thickness. This solution procedure provides the adherend level results (mid-plane displacements, strains, and curvatures and force and moment resultants) along the joint *x*-direction (see Figure 1). The ply level in plane stresses are then determined via Classical Lamination Theory, and the interlaminar stresses are calculated via integration of the equilibrium equations (see [18] for details).

Cases 1 – 3, considered herein, represent standard non-stepped and stepped double lap joints that were considered by Mortensen and Thompsen[4] and that have been included within the HyperSizer bonded joints capability for some time. Cases 4 and 5, in which one adherend is a honeycomb sandwich panel, could be analyzed using the standard double lap joint capability provided the core material is simply treated as a ply and the honeycomb sandwich panel treated as a laminate. However, it is also possible to treat the core material as an additional layer of normal and shear springs, similar to how the adhesives are treated in the formulation. This better captures the physics of the core behavior as it enables the core material to deform in the through-thickness direction. As such, a new sandwich double lap joint concept that treats the core as an additional adhesive was formulated and implemented within the HyperSizer joints capability.

Figure 3 here

The HyperSizer geometry for the Cases 5 and 6 joint is shown in Figure 3. The grids shown in the geometry details actually represent analysis points (locations where outputs are evaluated) in the model adherends (as opposed to elements typically shown for finite element models). In the *x*-direction, Regions 1 and 3 were divided into 25 segments, each with 5 points. In Region 2, each of the four steps were divided into 5 segments, each with 5 points. In the z-direction, 15 analysis points were used per ply. Again, these z-direction analysis points were used to determine the interlaminar stresses through numerical integration. The adhesives and core do not participate in this integration as they are modeled as distributed layers of normal and shear springs. Thus, three output points were used for the adhesive and core: one at the top and bottom and one in the middle.

C. Joint Element Designer (JED)

The Joint Element Designer (JED) software was originally created to integrate finite element software and semi-analytical joint models [5,19]. The model uses the same assumptions for the adherends as the HyperSizer method: beams under cylindrical bending, although the beams can be Euler-Bernoulli or Timoshenko with shear deformations. Multiple models have been implemented for the core/adhesive layers, with distinctions having to do with the interpolation of displacements through the thickness or the constitutive model. Linear interpolation through the thickness is generally used for adhesives due to their thin nature, while sandwich cores typically require higher order quadratic functions[20]. Though not utilized here, options such as nonlinear geometry (through co-rotational formulation), crack growth, adaptive shape functions, and graded adhesives are available[21–23]. The model utilizes a standard finite element solution procedure for beam elements, with a few key differences. Rather than polynomial functions chosen for shape functions along the axial axis, the structural model is solved using the matrix exponential[24]. This results in shape functions that are determined rather than prescribed. This means that a single element is sufficient for a joint with linear elastic materials as the shape functions are customized to the joint problem being considered. However, more elements may be needed along the length so improve solution stability. Finally, complex joints can be made by joining different elements at nodes like standard finite element software.

Since the HyperSizer method uses linear variation of displacements through the core/adhesive thickness, to draw more of a distinction, the JED model in this study used the quadratic variation of displacements through the adhesive/core. The displacements in the core (or adhesive), $w_c(x,z)$ and $u_c(x,z)$, are assumed to be in the form of:

$$u_c(x,z) = a_0(x) + z a_1(x) + z^2 a_2(x) \tag{1}$$

and

$$w_c(x,z) = b_0(x) + z b_1(x) + z^2 b_2(x) \tag{2}$$

where the functions $a_i(x)$ and $b_i(x)$ can be found in terms of the the displacements at the interface between the adherend above and below the adhesive/core (assuming perfect bonding) and the displacement of the adhesive/core centerline. Thus, the energy can be formulated in terms of centerline displacements, which are only unknown in x, and the system of ODEs can be solved. Additionally, for this model, the stresses in the adhesive/core were assumed to be uncoupled, meaning that

$$\mathbf{D_c} = \begin{bmatrix} E_{cxx} & 0 & 0 \\ 0 & E_{czz} & 0 \\ 0 & 0 & G_{cxz} \end{bmatrix} \tag{3}$$

where

$$\boldsymbol{\sigma_c} = \mathbf{D_c}\boldsymbol{\epsilon_c},$$

$$\boldsymbol{\sigma_c} = [\, \sigma_{cxx} \quad \sigma_{czz} \quad \tau_{cxz}]^{\mathrm{T}} \text{and } \boldsymbol{\epsilon_c} = [\, \epsilon_{cxx} \quad \epsilon_{czz} \quad \gamma_{cxz}]^T \tag{4}$$

Here, E_{cxx}, E_{czz}, and G_{cxz} are the elastic properties of the adhesive/core, whereas, σ_{cxx}, σ_{czz}, τ_{cxz}, ϵ_{cxx}, ϵ_{czz}, and γ_{cxz} are the stress and strain components of the adhesive/core.

While analyzing the sandwich joints (Cases 4-6), the combination of a thin adhesive layer and thick core in the same element caused instabilities due to vastly different magnitudes of eigenvalues in the coefficient matrix of the system of ODEs to be solved. Therefore, very small elements were needed in the x-direction in order to achieve a converged solution. Globally, a nominal element size of 0.01 in. was used, which translates to 226 elements total.

D. Carrera Unified Formulation (CUF)

One-dimensional Carrera Unified Formulation (CUF) decomposes the three-dimensional field into an axial displacement function $\boldsymbol{u_\tau}(x)$ along the beam axis and a cross-section expansion function $F_\tau(y,z)$ along the y-z plane[6]. Therefore, the generalized displacement field can be expressed as follows:

$$\boldsymbol{u}(x,y,z) = F_\tau(y,z)\boldsymbol{u}_\tau(x) \tag{5}$$

where the index τ corresponds to the expansion terms of the structural theory. Repeated indices denote summation as per Einstein notation which means τ is summed from 1 to M expansion functions. The choice of

F_τ defines the adopted structural theory and the current work adopts Lagrange polynomials as expansion function (LE)[25]. The component-wise (CW) modeling approach, an extension of LE models, allows modeling of multi-component structures through a compact and unique 1D formulation[26] and will be used throughout this study. Figure 4 illustrates the CW modeling approach adopted for Case 5. Different components of the adhesively bonded joint are decomposed into individual 1D beam elements and the compatibility along the interfaces of different components is enforced by superimposing the degrees of freedom associated with the given interface. Different cross-sectional expansion configurations are assigned to individual beams based on their design layout.

Figure 4 here

The standard finite element approach is adopted to discretize the beam axis along the *x*-direction, and the displacement field (Equation 5) can be reformulated as:

$$\boldsymbol{u} = F_\tau(y,z)N_i(x)\boldsymbol{u}_{\tau i} \qquad 6$$

where N_i is the i^{th} shape function of order p, $\boldsymbol{u}_{\tau i}$ is the generic finite element nodal vector, and i is summed from 1 to p+1. The choice of shape function N_i remains independent of the kind of expansion function F_τ. Using the principle of virtual work, the invariant form of the structural stiffness matrix is formulated as:

$$\delta L_{int} = \delta \boldsymbol{u}_{js} \int_V N_j(x)F_s(y,z)\boldsymbol{D}^T\boldsymbol{C}\boldsymbol{D}\,N_i(x)F_\tau(y,z)\boldsymbol{u}_{\tau i}dV = \delta \boldsymbol{u}_{js}\boldsymbol{k}_{ij\tau s}\boldsymbol{u}_{\tau i} \qquad 7$$

where $\boldsymbol{D}$ is the differential operator matrix of size 6 x 3, $\boldsymbol{C}$ is the constitutive material matrix and $\boldsymbol{k}_{ij\tau s}$ is the fundamental nucleus of the stiffness matrix of size 3 x 3, whose formal expression remains the same irrespective of the choice of shape function and expansion function. The indices (i,j) and (τ,s) correspond to the finite element nodes and expansion terms of the structural theory, respectively. Readers are referred to the book by Carrera and coworkers for detailed information on the formulation as well as implementation of CUF models[6]. CUF models are part of a suite of high-fidelity numerical models for solving a variety of structural problems including, but not limited to, progressive failure analysis in composite[27], large deflection and post buckling analysis[28], and global-local approach[29].

In this work, a sixteen node (L16) LE expansion function corresponding to a bi-cubic approximation is utilized for modeling various components within the cross-section. A four-node cubic beam element (B4) is employed to discretize the beam with varying mesh density, which is biased towards the vicinity of geometric and material discontinuities. All the components of the beam are modeled as continuum elements with a combination of L16-B4 configurations. Although not utilized in this study, the model also has the capability of modeling nonlinear adhesive layers using continuum damage[27] as well as cohesive elements[29].

E. Parametric Continuum Solid Shell (CSS) FE

A parametric 3-D finite element model was developed using the python scripting interface for Abaqus for the joint cases with a sandwich adherend. By automating the finite element modeling process from pre to post-processing, the script enables relatively quick evaluation of joints with varying parameters.

The model is intended to be fast running for preliminary design evaluations. Therefore, the mesh refinement and element type were chosen to balance run time and stress field fidelity as follows. The mesh is shown in Figure 5 colored by component. The doubler, adhesive, and facesheet were each modeled with one layer of continuum solid shell elements (CSS8) per ply. The continuum solid shell element is a formulated with seven incompatible modes to improve bending behavior and an assumed strain to mitigate locking[7,30]. The core was modeled with continuum solid elements with reduced integration (C3D8R) and enhanced hourglass control. The in-plane element edge length varied from 0.004 to 0.04 inches in the doubler region. In general, the mesh refinement used was found to be converged except immediately at the reentrant corners where stress singularities exist in linear analyses.

To facilitate comparison with the 2-D analysis methods, additional assumptions and approximations specific to this study were required. The dimension of the model along the joint axis (y-direction) was arbitrarily set to one inch and plane strain was assumed by enforcing zero y-direction displacement at all nodes. Linear analysis was conducted using Abaqus 2017.

Figure 5 here

F. Benchmark: High Fidelity FEM

In order to establish a reference for the various comparisons, full 3-D continuum mechanics finite element analyses with high mesh density were carried out using the commercial finite element analysis program Abaqus. The finite element meshes are shown in Figure 6. The objective for these models was to find 'converged' stress fields – time or computational efficiency were low priority. The metallic adherends, as well as the adhesive layers, were discretely modeled as isotropic, homogeneous continua. Individual plies were discretely modeled as transversely isotropic and orthotropic continua for unidirectional and fabric composite layers, respectively. Each ply had individual material orientations assigned to capture the ply stacking and anisotropic effects. Ply drops were idealized as abrupt steps.

Figure 6 here

Biased mesh generation in both the longitudinal and thickness direction was utilized. In order to capture high stress gradients, the mesh density in the proximity to geometric discontinuities in longitudinal direction, such as ply drops, and in proximity to material discontinuities in thickness direction, such as interfaces between individual plies, core, or adhesive materials, was increased. At least ten three-dimensional linear continuum mechanics reduced integration elements (C3D8R) were used through the thickness of each ply, adhesive layer or metallic adherend. At least 20 elements were used through the thickness of the core. The convergence of the mesh density through the thickness was judged by observing the transverse shear and normal stress continuity through the thickness at the center of the width of the joint at the characteristic distance 'inward' from both reentrant corners. The characteristic distance (half ply thickness) was chosen since it is a commonly used measure to step away from the stress singularity occurring at the edge of the reentrant corner. Similarly, the mesh density in joint longitudinal direction was judged by the continuity of the peel and shear stress along the adhesive centerline at half width and thickness. The aspect ratios of the elements were kept less than 1:4 in areas of high gradients to keep locking effects at a minimum.

Similar to the CSS finite element models, the width of the joint was arbitrarily chosen to be one inch. All nodes were restrained in width direction to simulate plane strain conditions. Loads and boundary conditions were introduced using reference points and kinematic coupling constraints such that the conditions could effectively be applied to the neutral axis of the adherends in addition to effectively maintaining "plane remains plane" (plate) conditions at the boundary.

4. Results

Results are presented in two forms: line plots and contour plots. The line plots show the stress along the centerline of the top adhesive layer. The peel (σ_{zz}) and shear (τ_{xz}) stresses are considered critical for the adhesive and are each plotted for the six cases in Figures 7, 9, 11, 13, 15, and 17. For the adherends, the axial stress (σ_{xx}) is the primary component. Additionally, delamination can be a major concern for composite adherends and the interlaminar stresses (σ_{zz} and τ_{xz}) have been considered. A contour plot of these stresses at critical regions for the six cases is presented in Figures 8, 10, 12, 14, 16, and 19. The results for each of the six cases are presented here, followed by a discussion of the results in the next section.

Figure 7 here

Figure 8 here

Figure 9 here

Figure 10 here

Figure 11 here

Figure 12 here

Figure 13 here

Figure 14 here

Figure 15 here

Figure 16 here

Figure 17 here

Figure 18 here

Figure 19 here

Figure 20 here

5. Discussion

A. Comparison of Joint Configurations

One can compare the six considered cases with one another and observe what effect incremental changes in joint configuration can have on the stress distributions. First, looking at the difference between Cases 1 and 2 shows not only the difference between using composite and homogenous materials, but materials with different stiffnesses. The bending stiffness (D_{11}) of Case 2 is 10% and 7% lower than Case 1 in the adherend and doubler respectively. Similarly, the axial stiffness (A_{11}) is 5% and 7% lower in the adherend and doubler. As a result, the stress magnitudes for almost all stresses were lower and generally in the adherend/doubler (Figures 8 and 10). Even the peel and shear stresses in the adhesive were lower for Case 2 as shown in Figures 7 and 9. This is particularly clear in the benchmark finite element peel stress results in the adhesive. The "trough" just before the stress begins to rise to the peaks are much lower in magnitude for Case 2. This is because the benchmark finite element model captures the effects of the 45° facesheet ply adjacent to the adhesive. The analytical models determine the adhesive stresses based on the homogenized adherend laminate properties and therefore do not capture these effects.

The effect of tapering the doubler can be seen by comparing Cases 2 and 3 and Cases 4 and 5. For the adhesive stresses, the taper decreases the peel and shear stress concentrations near the taper as would be expected. The stresses in the middle of the joint (x = 2.05 in.) do not appear to be heavily influenced by the taper, which for this particular joint is the critical region. In practice, inserts or gap fillers are applied in the gaps to lower the stress concentration, but this gap area remains a critical region. For the adherend/doubler stresses, the taper lowers the peak shear near the taper but has little impact elsewhere. There is an even more drastic reduction in interlaminar peel stress (σ_{zz}) due to the taper. The peak axial stresses didn't appear to be largely affected.

Similarly, comparing Cases 2 and 4 and Cases 3 and 5 can lead to general observations about the difference in stresses by adding a core. For adhesive stresses, the peel stress becomes slightly more concentrated in at the ends and even changes signs in the middle for the sandwich joints from tension to compression. The adhesive shear stress is more spread out for the sandwich joints, but the magnitude of the peak is not greatly impacted. For the adherend stresses, the sandwich cases generally had lower out-of-plane stresses. This is to be expected, because the core is relatively soft in shear and transversely, which relieves much of the peel and shear stress built up in the adherend/doubler of the non-sandwich joints. The adherend/doubler axial stresses seem to be a bit higher for the sandwich cases, but not drastically.

B. Discussion of A4EI

The A4EI results reflect the fact that this legacy tool is considerably more limited than the other analysis tools included in the study. A4EI does not predict adhesive peel stresses nor the stress fields in the adherends, and thus A4EI results can only be compared for the adhesive shear stress. In addition, the shear loading of Case 6 cannot be applied in A4EI, so no results are shown for the tool in that case. The adhesive shear stress predicted by A4EI is in reasonably good agreement with the benchmark FEA and the other tools. As with JED and HyperSizer, A4EI's non-continuum spring representation of the adhesive does not allow it to predict the reversals in the shear and peel stress at the free edge that are predicted by the benchmark FEA. In the cases with

the core, A4EI overpredicts the peak adhesive shear stress at the right edge. This tendency to be conservative might explain why the tool has been successfully employed for bonded joint design for many years despite not providing any of the details of the other tools considered herein.

C. Discussion of HyperSizer

For most of the cases examined, JED and HyperSizer produced very similar results, and both are in reasonably good agreement with the benchmark solution. This is due to similar underlying assumptions of beam-like behavior for the adherends and distributed springs to represent the adhesive and core. The benchmark finite element analysis, in contrast, is a full continuum solution, which illustrates some effects not captured by the more simplified models. Of particular interest is the behavior of the transverse shear stress τ_{xz} at the re-entrant corners of the cases studied. The benchmark solution clearly demonstrates that this τ_{xz} traction must equal zero at the free edge (of both adherends and adhesives), whereas neither HyperSizer nor JED enforce this behavior at free edges normal to the x-direction. The result is, at times, appreciably higher peak stresses at the edges predicted by the simplified tools in both τ_{xz} and σ_{zz}, the latter of which being affected by the former.

In Case 1 (Figure 7 and Figure 8), the in-plane σ_{xx} appears to vary quadratically through the thickness of the center adherend in the benchmark case, while being represented as constant through the thickness for JED and HyperSizer. Both of the rapid tools use classical lamination theory assumptions of linear in-plane stresses through the thickness of each ply. In the case of a single "ply" with no bending (as in Case 1 center adherend), the result is a constant through-thickness σ_{xx}. For both Cases 1 and 2 (Figure 7 - Figure 10) , the lower-order representation of σ_{xx} results in some differences in the details of the derived τ_{xz} and σ_{zz} fields when compared to the benchmark FEA. It is also of note that the over-prediction of the peak τ_{xz} and σ_{zz} in the adhesive (and related under-prediction of the "trough" prior to the peak in the adhesive σ_{zz}) is much greater in the Case 2, in which the adherends are composites rather than isotropic aluminum. This is because, as mentioned previously, the HyperSizer method cannot capture the effect of the compliant 45° facesheet ply adjacent to the adhesive.

For Case 3 (Figure 11 and Figure 12), although both JED and HyperSizer capture the effect of the moment introduced at ply drop locations, they overpredict the peak stresses and re-entrant corner τ_{xz} and σ_{zz}. This difference is again due to the benchmark FEA capturing the zero τ_{xz} at x-direction free-edges, whereas this cannot be achieved for the other tools. Still, both JED and HyperSizer do quite a good job of reproducing the benchmark FEA stress fields.

Cases 4 and 5 (Figure 13 - Figure 16) exhibit the same free-edge τ_{xz} effects noted for Case 3, but also demonstrate the impact of core compliance. The HyperSizer solution treats the core as an additional adhesive, resulting in zero core σ_{xx}, constant τ_{xz}, and linear σ_{zz} through the core thickness. In contrast, the employed JED formulation results in quadratic σ_{zz} through the core thickness. FEA, being a continuum solution with high density piecewise linear approximations of shape and displacements in either direction, may produce more complex distributions in both the core and the adherends. For example, for Case 4, HyperSizer matches the stresses in the adhesive quite well, but misses the reversal just adjacent to the free right edge (see Figure 13). Examining the Case 4 stress fields in this vicinity (Figure 14), HyperSizer predicts a positive τ_{xz} peak in the top facesheet at the right free edge. In reality, τ_{xz} is a traction at this free edge and must be zero. The benchmark FEA captures this as, when approaching the right free edge in the top facesheet, the τ_{xz} first rises slightly and then rapidly approaches zero. In HyperSizer, the adherend σ_{zz} is calculated by integrating $d\tau_{xz}/dx$ (see ref [17]), therefore, directly at the right free edge of the top facesheet, HyperSizer predicts compressive σ_{zz}, whereas the benchmark FEA indicates that this stress is tensile. It should be noted, however, that, in practice, the joint geometry will not match the idealized geometry employed by any of the tools. Particularly at a free edge in the vicinity of the bondline, imperfections and features like the spew filet will influence these very local stress features described above.

Case 6 (Figure 17 - Figure 20) was chosen to be quite challenging for the HyperSizer solution. The loading mimics three-point bending, but the aspect ratio of the joint is approximately 4:1, thus the simulation is actually closer to short beam shear. The HyperSizer formulation is based on plates in bending connected by continuous normal and shear springs. Furthermore, the load path is through the core (which is usually avoided in practice), further amplifying the impact of the core formulation. That being said, HyperSizer still does a decent job of reproducing the benchmark FEA stresses, particularly for the top of the joint in the vicinity of the load application. In concordance with the previous cases, HyperSizer still over predicts the peak stresses and predicts a peak τ_{xz} at the right free edge of the top facesheet. At the right bottom of the joint, the disparity

between HyperSizer and the benchmark FEA is greater. Examining the σ_{xx} fields predicted by the benchmark FEA in this vicinity (Figure 18), it is interesting that the z-direction distribution of σ_{xx} in the free hanging portion of the bottom adherend is opposite of what one would expect if the joint were dominated by bending. That is, the peak tensile σ_{xx} is at the top face rather than the bottom face. HyperSizer, on the other hand, predicts the trend that would be expected based on its bending formulation. This difference in σ_{xx} then results in further discrepancies in the τ_{xz} and σ_{zz} predicted by HyperSizer near the bottom right of the joint. However, examining the stress fields throughout the joint in Case 6, HyperSizer generally still does quite a good job of reproducing the benchmark FEA results.

D. Discussion of JED

The previous discussion on the HyperSizer model is mostly applicable for the JED model as well. One of the main differences is the quadratic distribution of the adhesive/core displacements in the z-direction. This difference means that the adhesive shear stress falls to near zero at the ends of the adhesive (see for example Figure 9), and the peel stress rises near the reentrant corner (top corner of the adhesive) and falls in the other direction (bottom corner of adhesive). Since the out-of-plane stresses are calculated based on integrating from the stress state of the neighboring adhesive, the extreme stress gradient at the corners results in large stresses in the doubler (see for example τ_{xz} and σ_{zz} for Case 4, Figure 14).

E. Discussion of CUF

The CUF model performs well in comparison to the benchmark solution for all six cases. Good agreement can be observed with the benchmark solution for the distribution of adhesive peel and shear stresses. Certain shear stress τ_{xz} contour plots (such as τ_{xz} in Figure 8) exhibit slight discontinuity at the interface because CUF models are displacement-based formulations which do not guarantee stress continuity. Such shortcomings can be alleviated through a mixed formulation such as Reissner's mixed variational theorem[31]. In addition, CUF models are post-processed at nodal points using the strain-displacement relations based on the structural theory and the material constitutive law rather than interpolation based on the surrounding Gauss points (a default procedure in commercial software). The piecewise-cubic kinematic approximation incorporated within the CUF models can accurately capture the stress reversals observed along free surfaces, such as τ_{xz} in Case 5 (Figure 15). It can also be observed that CUF results are consistent with the benchmark solution in capturing the traction-free conditions of τ_{xz} at free surfaces for all six cases. A slight trough in adhesive stress before peaking is observed in Case 1 and Case 2 (Figure 7 and Figure 9). The lowering of the peak due to the presence of 45° ply in Case 2 is accurately captured by CUF. Predictions of stress peaks at ply drop locations can also be observed for Case 3, Case 5 and Case 6 (Figure 11, Figure 15 and Figure 17) and are consistent with the benchmark solution. In Case 6 the loading conditions emulate three-point bending, thereby leading to significant shear deformation in the core. In contrast to the analytical models, the cubic kinematic approximation of the core in CUF tends to capture the stress gradients without any abnormally high stress gradients in the vicinity of corners and the corresponding core and facesheet (Figure 19 and Figure 20). The requirement of multiple linear elements along the thickness to capture transverse distribution combined with aspect ratio constraints can severely increase the computational size in benchmark models whereas the 1D finite element analysis combined with high-order approximation of CUF nullifies such aspect ratio constraints.

F. Discussion of CSS FE

The CSS FE model performed very well as compared with the benchmark results for the three cases in which it was exercised (Cases 4, 5, and 6). Generally good agreement with the benchmark FEA was expected since the two models are similar in many respects, with the main differences being the discretization and element types. For Case 4, the adhesive stresses showed excellent quantitative agreement with the only discrepancies being located immediately at the reentered corners (see Figure 13). Since CSS FE mesh included a single element through the thickness of the adhesive, it was unable to predict the stress reversals in τ_{xz} and σ_{zz} in the adhesive near the free edge. The contour plots show very good agreement with the benchmark results in general. Minor differences are noted in σ_{xx} and τ_{xz} in the composite facesheets as compared with the benchmark FEA. In cases where the CSS FE differs from the benchmark it appears to be in good agreement with HyperSizer and JED, likely due to the relatively coarse (as compared to the benchmark) approximation of the continuum solution afforded by using one CSS8 element per ply. Cases 5 and 6 exhibit similar features as Case 4 in terms of the comparison of the CSS FE with the benchmark. In some cases the stress is overpredicted (e.g., peak values of σ_{zz} near the reentered corner) whereas in other cases the stress is underpredicted (e.g., τ_{xz} and σ_{zz} at

ply terminations). Although the model generally predicts the stress fields accurately, the locations where differences between the CSS FE results and the benchmark results occur are the hotspot locations where local minimum margins would be calculated for the purpose of design. Therefore, careful selection and interpretation of the stress fields and peaks is required.

A simplification of the CSS FE model where the composite facesheets and doublers were each modeled with one layer of continuum solid shell elements through the thickness was also explored for Case 4. The plies in the facesheet and doubler were represented using a composite section definition with three integration points per ply. Comparison of the results from the two versions of the model highlights the effect of treating the laminates like beams (as is done by HyperSizer and JED) vs. continuum on the adhesive stresses as show in Figure 21a. The shear stress predicted in the adhesive agrees with HyperSizer and JED predictions when one element through the thickness of the laminates is used. When one element per ply is used, the shear stress in the adhesive matches the benchmark result. The same trends were found for the peel stress and for the other cases. The stress fields in the adherends show a starker contrast between the two versions of the CSS FE model. Since the continuum solid shell elements assume a constant peel and shear strain through the thickness, simplifying the model to one element through the thickness of the laminate yields in a significant loss of fidelity in the adherend stress shear and peel fields as shown in Figure 21b. Therefore, in most cases, simplifying to one continuum solid shell element per laminate appears invalid.

Figure 21 here

G. Comparing Peak Adhesive Stresses

One aspect worthy of discussion is the comparison of adhesive stresses near the stress concentrations. The continuum-based FE models have stresses that vary through the thickness of the adhesive and stress singularities at the reentrant corner, which can never be resolved with a refined mesh. Meanwhile, spring-based models like the HyperSizer and JED models do not have the problem of stress singularities since the adhesive is given an interpolation function through the thickness (linear for HyperSizer, quadratic for JED) and do not enforce stress-free boundary conditions at the ends of the adhesive. To compare these two types of models is problematic at best, and tradition has dictated that stresses at the centerline of the continuum models are used for the comparison, although continuum-based FE models show that there is a strong stress gradient through the thickness at the ends of the adhesive, which makes the comparison somewhat arbitrary. The root of the problem lies in the fact that the most critical point of the adhesive is the point at which a rigorous comparison cannot be made.

To overcome this limitation and to dispel some of the ambiguity of stresses in this region, many have used the concept of a “characteristic distance”. In this approach, the stresses are compared at a characteristic distance from the edge, with one of many definitions of this distance being the thickness of a ply. For the cases shown here, the distance would be around 0.007 in., and some cases look like the stresses are independent of edge effects at the distance (for example Figure 13) but for others, the stress predictions have already diverged due to the boundary (Figure 11). This may be a good example of why using the characteristic distance for comparing continuum-based FE models with spring-based models may be problematic.

Furthermore, the characteristic distance has been used to predict strength for spring-type design models such as the HyperSizer or JED models. In this approach, a joint is tested experimentally, and based on the failure load a characteristic distance is found such that the predicted ultimate strength correlates with the test result. This is then used for other joints of the same material, with the characteristic distance considered to be a material property. One of the lessons of this study should be the that such methods should be considered with caution.

6. Conclusions

This study compared five bonded joint design tools with a benchmark high fidelity FE model for six different joint configurations. Three of the design models were ODE-based models (A4EI, HyperSizer, and JED), where beam theory and springs were used for the through-thickness interpolation of displacements, and the structural response was found by solving equilibrium in the axial direction. The fourth model is based on hierarchical higher-order one-dimensional theory (CUF) formulated within the scheme of the finite element method. The fifth model (CSS FE) was an automated coarse-mesh FE model with continuum elements for the adhesive/core and solid shell elements for the adherends. The six different joint configurations were derived from one joint configuration with a bonded sandwich panel under axial compression loading (Case 5), with

Case 6 being the same configuration under bending, and the other four configurations derived by removing either the doubler stepped ply drop (Case 4, Case 2), sandwich core (Case 3 and 2) , or layered composite adherends (Case 1).

The capabilities of A4EI are considerably fewer than the other tools, and it is able only to predict the adhesive shear stress for inclusion in the comparisons. These comparisons showed that A4EI's adhesive shear stress prediction was reasonable, but not in as good agreement with the benchmark solution as the other design tools. Generally speaking, all of the other models were able to represent the stresses in the adhesive and adherend/doubler fairly consistently and accurately. When discrepancies arose, they were typically found in the regions of the reentrant corners, which are always problematic and, unfortunately, the most critical. The fact that the JED and HyperSizer models do not enforce traction-free boundaries for the core/adhesive meant higher stresses at the ends of the adhesive than the benchmark. Similarly, the CSS FE model only represented the adhesive with one element, which could not resolve the traction-free boundary either and matched up closely with the other models.

For the adherend stress predictions, discrepancies with the benchmark were due to the assumption of displacement variation through the thickness. HyperSizer and JED assume linear axial displacements through the thickness, and the CSS FE model assumes the same when one element through the adherend thickness is used. The error arising from this limitation were demonstrated by running the CSS FE model for one integrated layered element over the adherend thickness vs. one element per ply. The model with one element per ply showed much better agreement with the benchmark. Similarly, the CUF model uses a user-specified, higher order interpolation through the thickness of the adherend, which results in agreement similar to the CSS FE model.

Although adherend through-thickness stresses are assumed to be negligible for beam theory, an equilibrium-based approach for finding these stresses has been implemented in HyperSizer and JED with the results presented throughout the paper. The out of plane stress, σ_{zz}, is based on through-thickness integration of the x-derivative of the shear stress, τ_{xz}, making it sometimes sensitive to grid spacing.

The interpolation of displacements within the core and adhesive layers was another source of error. The HyperSizer model used linear interpolation, while the JED model used a quadratic interpolation. For Cases 1-5, this did not appear to make much of a difference other than the fact that the shear stresses for the JED model went near zero at the ends of the adhesive. However, when shear in the core was the dominant mode as in Case 6, the core was not sufficiently represented with linear displacements and larger discrepancies with the benchmark resulted.

Although there are discrepancies between the design models and the benchmark, it is important to keep two things in mind. 1) It is very unlikely that joints in practice have completely sharp re-entrant corners and ply drops, which lead to a stress singularity in models, so spending effort to resolve this difference may not be worthwhile. 2) These models are design models, so they are built for speed rather than purely for accuracy. The design models all had runtimes in the order of seconds to minutes, orders of magnitudes faster than the benchmark. The ranking of runtimes of the design models appeared to be inversely proportional to the ranking of model accuracy, although this was not rigorously assessed. Additionally, when evaluating runtime, one must also consider pre and post processing time, which can dwarf processing time. All of the design models featured here have been automated in some form with easy and clear methods for extracting results. Therefore, as long as limitations highlighted here are kept under consideration, these design models can enable parametric studies, sizing studies, and joint configuration comparisons for adhesively bonded joints.

7. Acknowledgements

The authors acknowledge the support from the Space Technology Mission Directorate Composite Technologies for Exploration Project and the Aeronautics Research Directorate Transformational Tools and Technologies Project. The Politecnico di Torino authors acknowledge funding from the European Union Horizon 2020 Research and Innovation program under the Marie Skłodowska-Curie grant agreement No. 642121 under framework of project FULLCOMP (FULLy analysis, design, manufacturing, and health monitoring of COMPosite structures). The authors have no conflict of interest regarding this research.

8. References

[1] Samantha Bell, "Structural adhesives deliver lighter composite structures with performance and costs benefits," *Reinforced Plastics*, Feb. 2012.

[2] Hart-Smith, L. J., "Adhesive-bonded single-lap joints," *NASACR112236*, 1973, p. 116.

[3] Hart-Smith, L. J., *Adhesive-bonded double-lap joints. [analytical solutions for static load carrying capacity]*, 1973.

[4] Mortensen, F., and Thomsen, O. T., "Analysis of adhesive bonded joints: a unified approach," *Composites Science and Technology*, vol. 62, Jun. 2002, pp. 1011–1031.

[5] Stapleton, S. E., and Waas, A. M., *The Analysis of Adhesively Bonded Advanced Composite Joints Using Joint Finite Elements*, Cleveland, OH: NASA Glenn Research Center, 2012.

[6] Carrera, E., Cinefra, M., Zappino, E., and Petrolo, M., *Finite Element Analysis of Structures Through Unified Formulation: Carrera/Finite*, Chichester, UK: John Wiley & Sons, Ltd, 2014.

[7] Smith, M., *ABAQUS/Standard User's Manual, Version 2017*, Providence, RI: Simulia, 2016.

[8] Stapleton, S. E., Bergan, A., Sleight, D. W., Bednarcyk, B. A., Zahn, A., Farrokh, B., Segal, K. N., Stier, B., and Jones, S., "Comparison of Design Tools for Stress Analysis of Adhesively Bonded Joints," *AIAA Scitech 2019 Forum*, San Diego, California: American Institute of Aeronautics and Astronautics, 2019.

[9] Wanthal, S., "Verification and Validation Process for Progressive Damage and Failure Analysis Methods in the NASA Advanced Composites Consortium," West Lafayette, IN, United States: 2017.

[10] Man, M., *Cytec Cycom 5320-1 T650 3k-PW Fabric Qualification Material Property Data Report*, Witchita, KS: National Institute for Aviation Reserach, 2015.

[11] "PAMG-XR1 5056 Aluminum Honeycomb, Rev 6.19.18," 2018.

[12] Leone, F. A., Dávila, C. G., and Girolamo, D., "Progressive damage analysis as a design tool for composite bonded joints," *Composites Part B: Engineering*, vol. 77, Aug. 2015, pp. 474–483.

[13] Hart-Smith, L. J., Company, D. A., and Center, L. R., *Analysis and design of advanced composite bonded joints*, National Aeronautics and Space Administration, 1974.

[14] *HyperSizer*, Collier Research Corp., https://hypersizer.com/, 2018.

[15] Yarrington, P., Zhang, J., Collier, C., and Bednarcyk, B., "Failure Analysis of Adhesively Bonded Composite Joints," Austin, Texas: American Institute of Aeronautics and Astronautics, 2005.

[16] Yarrington, P., Collier, C., and Bednarcyk, B., "Failure Analysis of Adhesively Bonded Composite Joints via the Virtual Crack Closure Technique," *47th AIAA/ASME/ASCE/AHS/ASC Structures, Structural Dynamics, and Materials Conference*, American Institute of Aeronautics and Astronautics, .

[17] Bednarcyk, B., Bansal, Y., Collier, C., Pindera, M.-J., and Zhang, J., "Analysis Tools for Adhesively Bonded Composite Joints, Part 1: Higher-Order Theory," *AIAA Journal*, vol. 44, 2006, pp. 171–180.

[18] Zhang, J., Bednarcyk, B. A., Collier, C. S., Yarrington, P. W., Bansal, Y., and Pindera, M.-J., "Analysis Tools for Adhesively Bonded Composite Joints, Part 2: Unified Analytical Theory," *AIAA Journal*, vol. 44, Aug. 2006, pp. 1709–1719.

[19] Stapleton, S. E., Waas, A. M., and Bednarcyk, B. A., "Bonded Joint Elements for Structural Modeling and Failure Prediction," *52nd AIAA/ASME/ASCE/AHS/ASC SDM Conference*, Denver, CO: 2011.

[20] Frostig, Y., Baruch, M., Vilnay, O., and Sheinman, I., "High-Order Theory for Sandwich-Beam Behavior with Transversely Flexible Core," *Journal of Engineering Mechanics*, vol. 118, 1992, pp. 1026–1043.

[21] Stapleton, S. E., Waas, A. M., Arnold, S. M., and Bednarcyk, B. A., "Corotational Formulation for Bonded Joint Finite Elements," *AIAA Journal*, vol. 52, 2014, pp. 1280–1293.

[22] Stapleton, S. E., Weimer, J., and Spengler, J., "Design of functionally graded joints using a polyurethane-based adhesive with varying amounts of acrylate," *International Journal of Adhesion and Adhesives*, vol. 76, Jul. 2017, pp. 38–46.

[23] Stapleton, S. E., Waas, A. M., and Arnold, S. M., "Functionally graded adhesives for composite joints," *International Journal of Adhesion and Adhesives*, vol. 35, Jun. 2012, pp. 36–49.

[24] Moler, C., and Van Loan, C., "Nineteen Dubious Ways to Compute the Exponential of a Matrix, Twenty-Five Years Later," *SIAM Review*, vol. 45, 2003, p. 3.

[25] Carrera, E., and Petrolo, M., "Refined beam elements with only displacement variables and plate/shell capabilities," *Meccanica*, vol. 47, Mar. 2012, pp. 537–556.

[26] de Miguel, A. G., Kaleel, I., Nagaraj, M. H., Pagani, A., Petrolo, M., and Carrera, E., "Accurate evaluation of failure indices of composite layered structures via various FE models," *Composites Science and Technology*, vol. 167, Oct. 2018, pp. 174–189.

[27] Kaleel, I., Petrolo, M., Waas, A. M., and Carrera, E., "Micromechanical Progressive Failure Analysis of Fiber-Reinforced Composite Using Refined Beam Models," *Journal of Applied Mechanics*, vol. 85, Dec. 2017, p. 021004.

[28] Pagani, A., and Carrera, E., "Large-deflection and post-buckling analyses of laminated composite beams by Carrera Unified Formulation," *Composite Structures*, vol. 170, Jun. 2017, pp. 40–52.

[29] Petrolo, M., Nagaraj, M. H., Kaleel, I., and Carrera, E., "A global-local approach for the elastoplastic analysis of compact and thin-walled structures via refined models," *Computers & Structures*, vol. 206, Aug. 2018, pp. 54–65.

[30] Vu-Quoc, L., and Tan, X. G., "Optimal solid shells for non-linear analyses of multilayer composites. I. Statics," *Computer Methods in Applied Mechanics and Engineering*, vol. 192, Feb. 2003, pp. 975–1016.
[31] de Miguel, A. G., Carrera, E., Pagani, A., and Zappino, E., "Accurate Evaluation of Interlaminar Stresses in Composite Laminates via Mixed One-Dimensional Formulation," *AIAA Journal*, vol. 56, Sep. 2018, pp. 4582–4594.

9. Tables

Table 1. Aluminum properties (all notional)

Property	Value	Units
E_{11}	10.0	Msi
E_{22}	10.0	Msi
E_{33}	10.0	Msi
G_{12}	3.85	Msi
ν_{12}	0.300	-
G_{13}	3.85	Msi
G_{23}	3.85	Msi
ν_{23}	0.300	-
ν_{13}	0.300	-

Table 2. Average IM7 / 8552-1 ply properties[9]

Property	Value	Units
E_{11}	21.3	Msi
E_{22}	1.26	Msi
E_{33}	1.26	Msi
G_{12}	0.749	Msi
ν_{12}	0.320	-
G_{13}	0.749	Msi
G_{23}	0.435	Msi
ν_{23}	0.450	-
ν_{13}	0.320	-
t_{ply}	0.0072	in

Table 3. Plascore 3/16" 3.1 pcf Honeycomb Core (PAMG-XR1 5056) properties[11]

Property	Value	Units
E_{11}	100*	psi
E_{22}	100*	psi
E_{33}	97000	psi
G_{12}	100*	psi
ν_{12}	0.5+	-
G_{13}	45000	psi
G_{23}	20000	psi
ν_{23}	0.001*	-
ν_{13}	0.001*	-
t_{core}	1	in

* Notional, assumed to be low

+ Assumed incompressibility in this plane

Table 4. Average T650 / 5320-1 plain weave ply properties[10]

Property	Value	Units
E_{11}	9.28	Msi
E_{22}	9.28	Msi
E_{33}	1.26*	Msi
G_{12}	0.735	Msi
ν_{12}	0.053	-
G_{13}	0.592+	Msi
G_{23}	0.592+	Msi
ν_{23}	0.106‡	-
ν_{13}	0.106‡	-
t_{ply}	0.0077	in

* Assumed to be equal to E_{33} for the IM7 / 8552-1 system
+ Assumed equal to the average of IM7 / 8552-1 G_{12} and G_{23}
‡ Assumed to be equal to $2\nu_{12}$

Table 5. Film adhesive properties (all notional)

Property	Value	Units
E_{11}	234000	psi
E_{22}	234000	psi
E_{33}	234000	psi
G_{12}	87800	psi
ν_{12}	0.330	-
G_{13}	87800	psi
G_{23}	87800	psi
ν_{23}	0.330	-
ν_{13}	0.330	-
$t_{adhesive}$	0.005	in

10. Figures

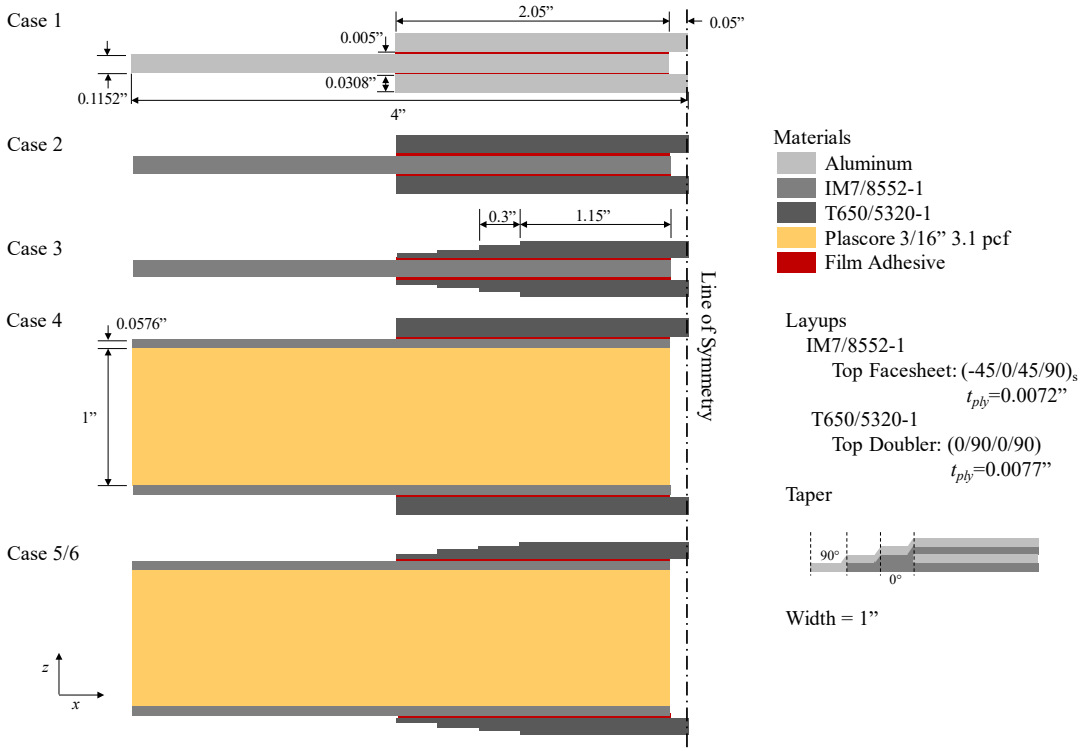

Figure 1. Geometry, materials, and layup of the six cases used to compare the design models.

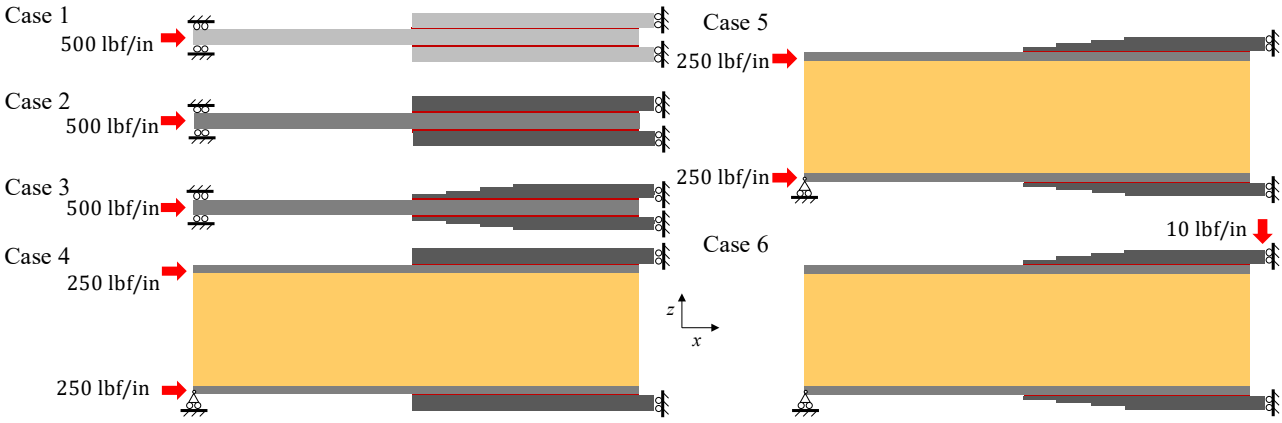

Figure 2. Boundary conditions for six cases used to compare the design models.

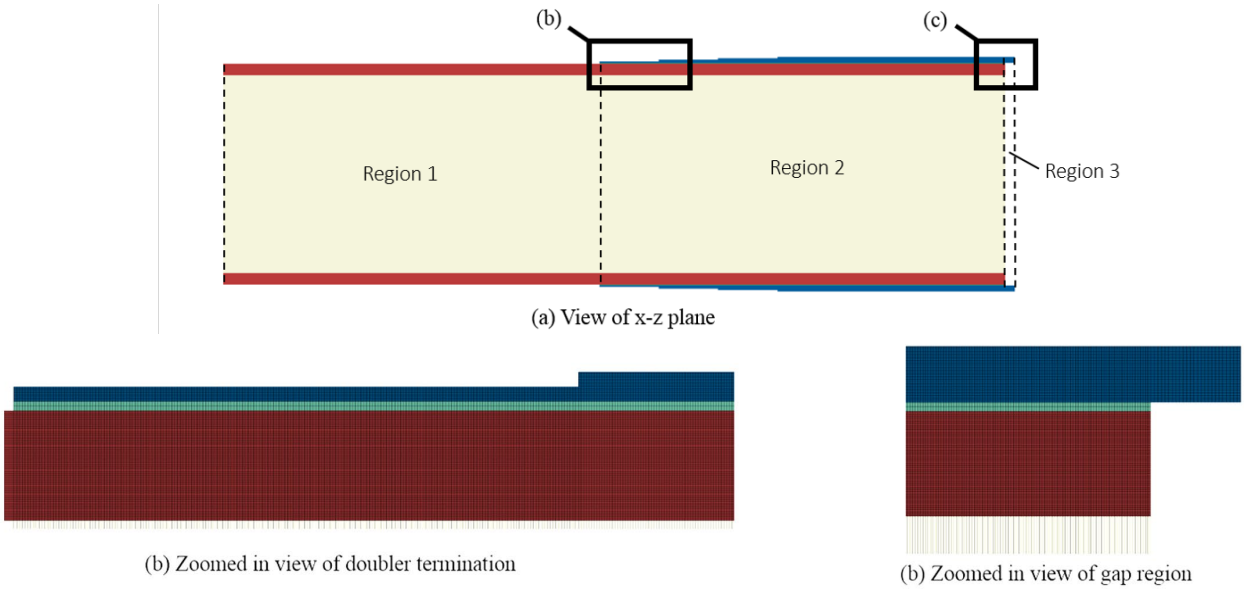

Figure 3. HyperSizer bonded joint analysis geometry for Case 5.

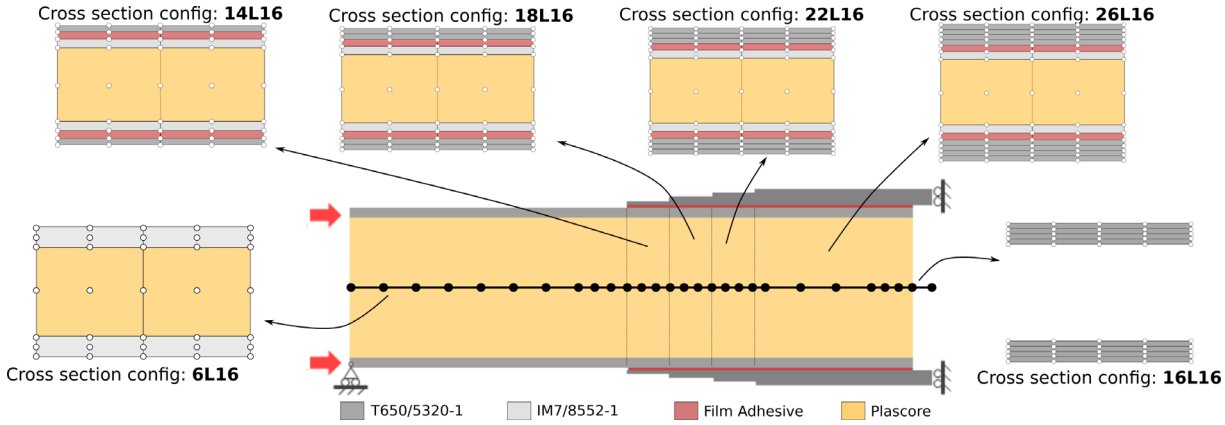

Figure 4. Illustration of component-wise modeling for CUF model for Case 5

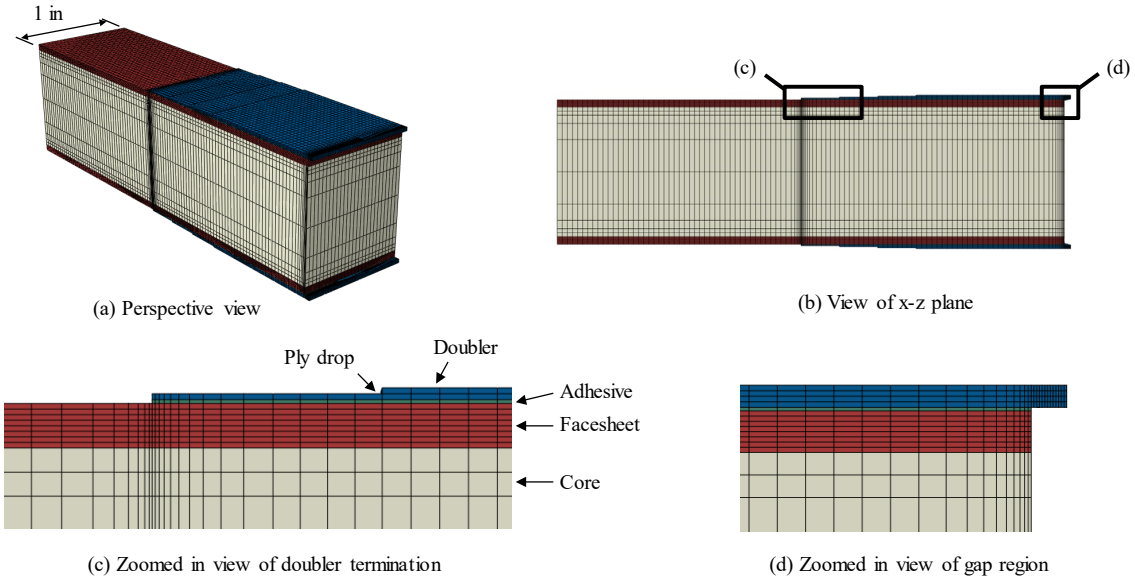

Figure 5. Parametric continuum solid shell FEM

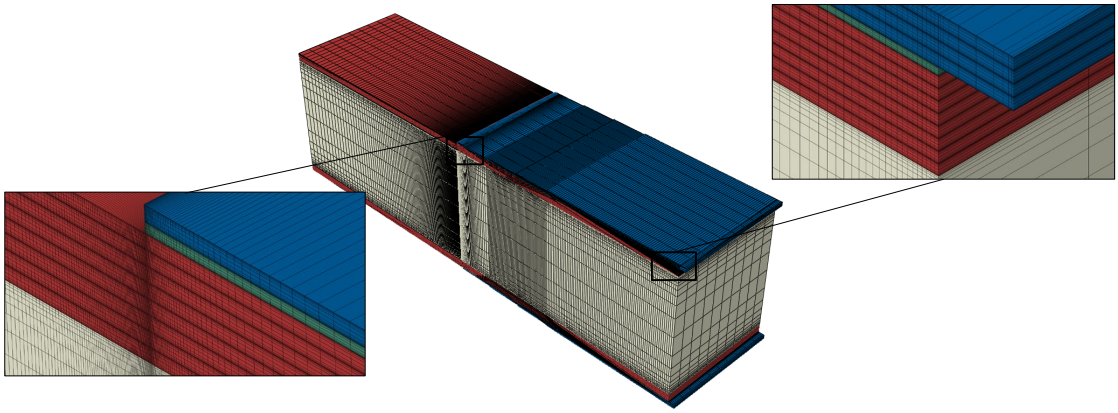

Figure 6. High Fidelity FEM used as a benchmark, showing details of the mesh at regions of highest refinement.

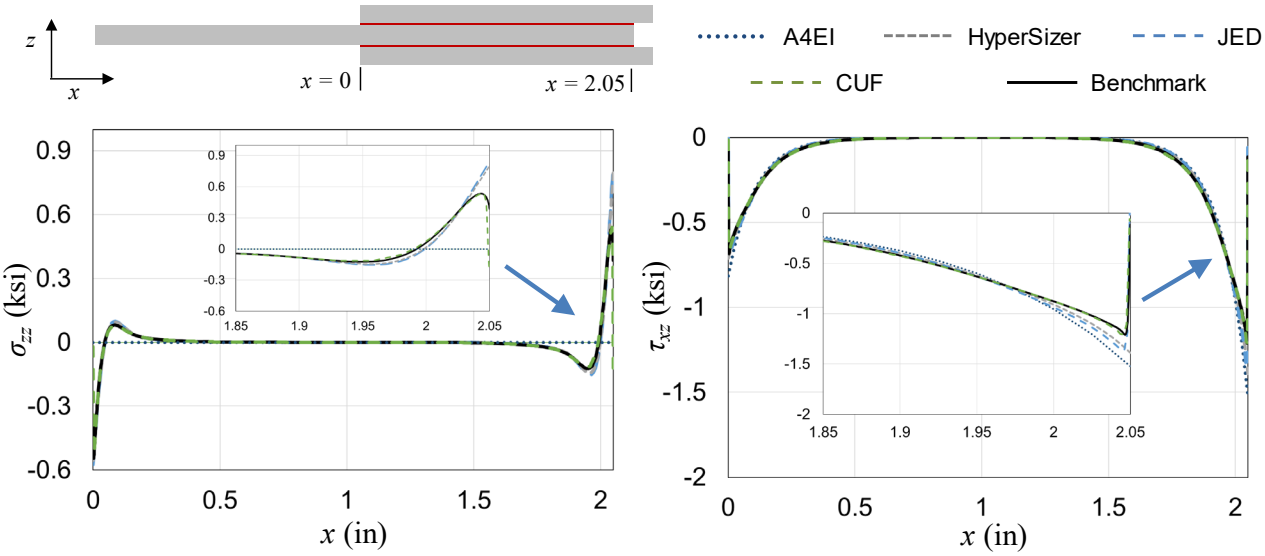

Figure 7. Peel (left) and shear (right) stresses along the top adhesive centerline of Case 1.

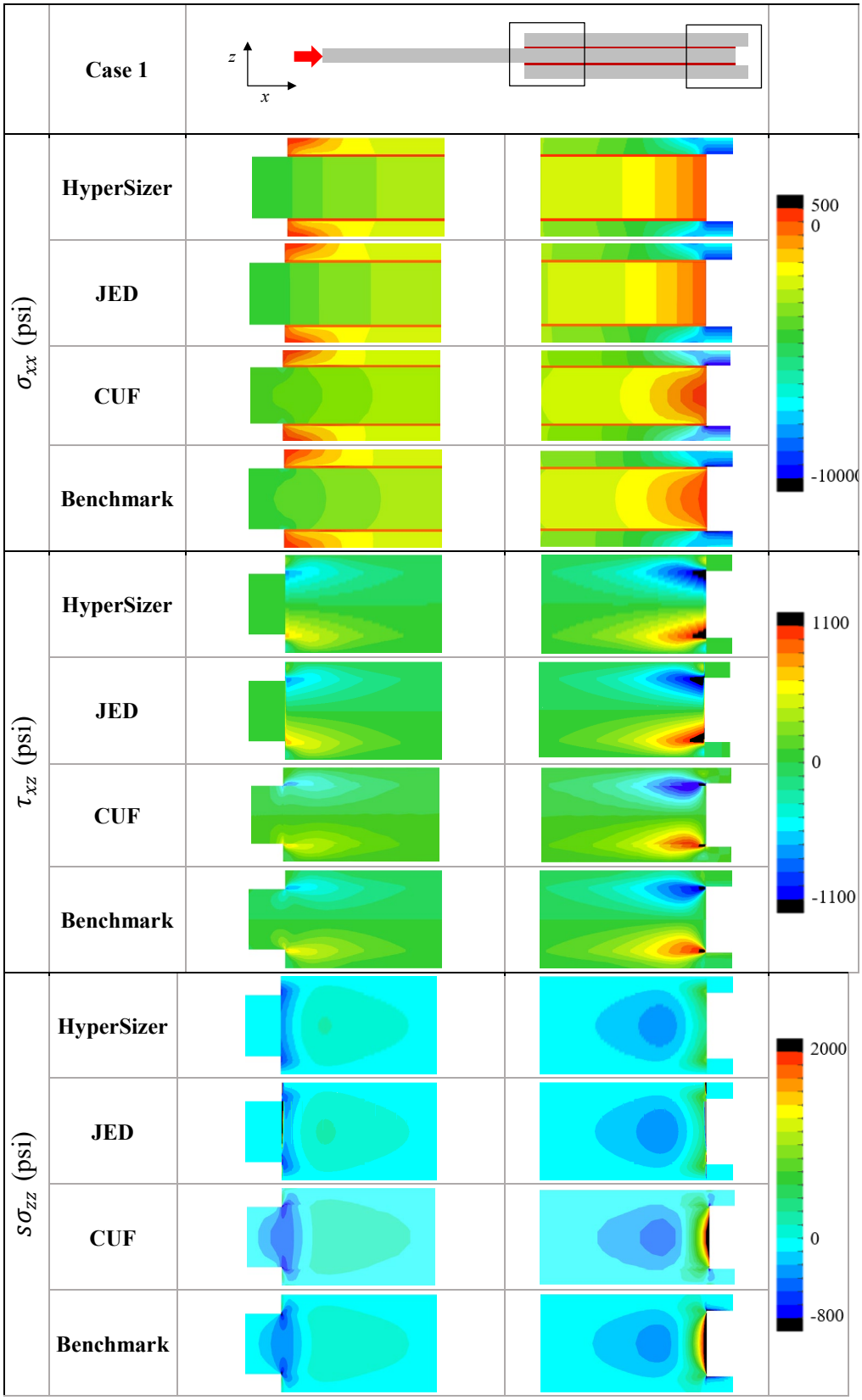

Figure 8. Axial, out-of-plane, and shear stress contours for Case 1.

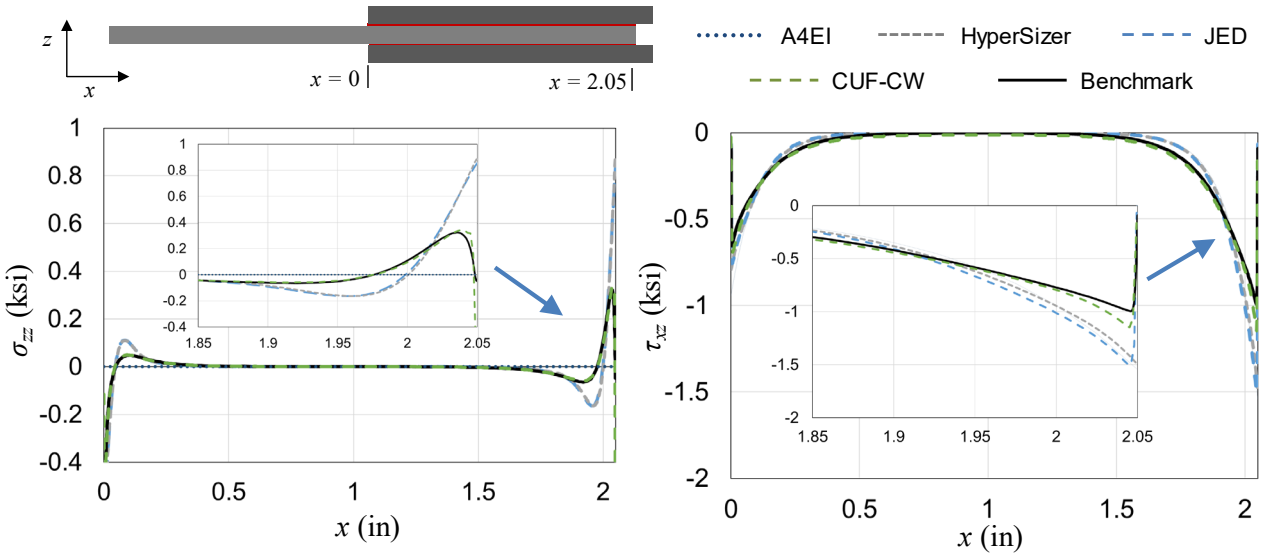

Figure 9. Peel (left) and shear (right) stresses along the top adhesive centerline of Case 2.

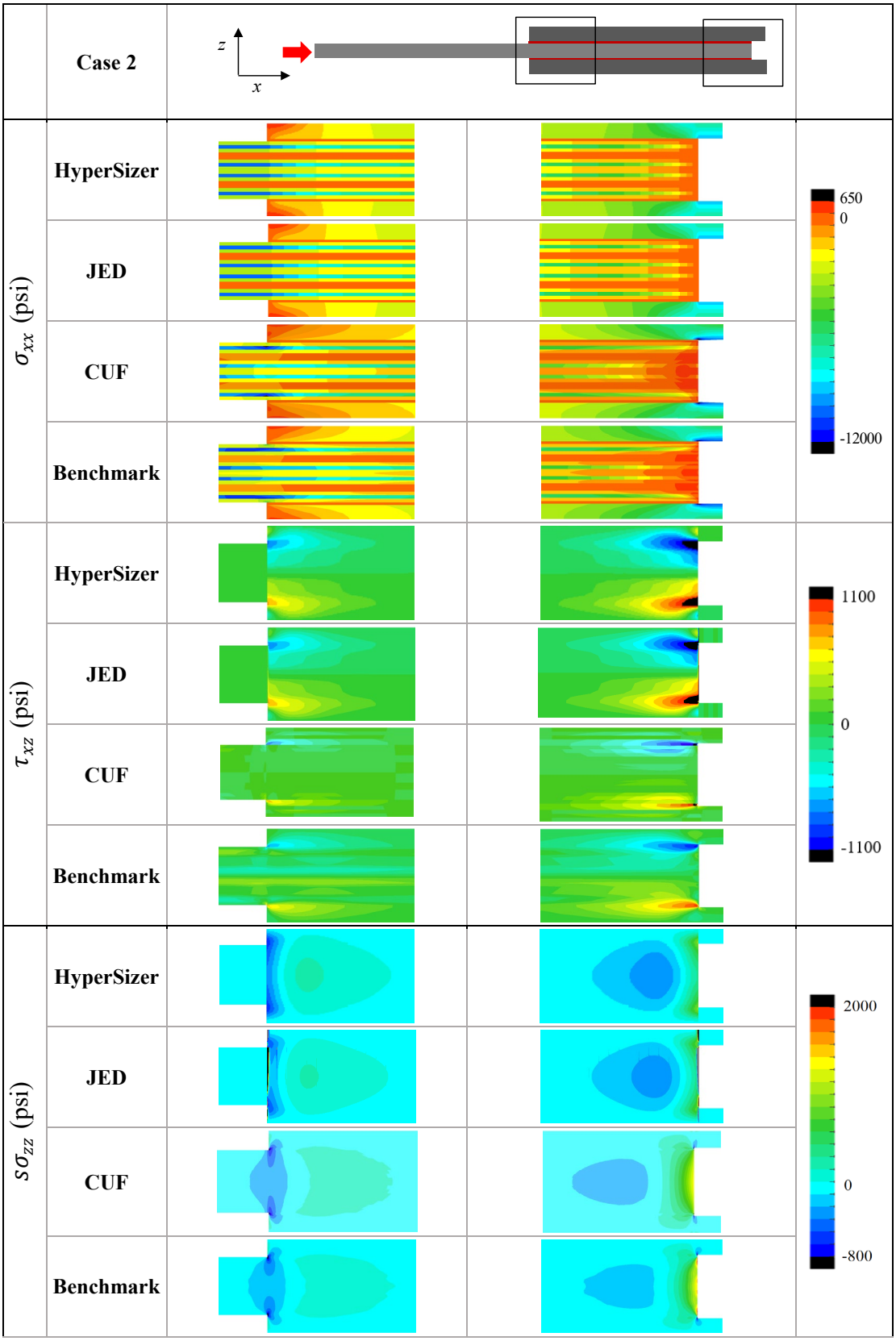

Figure 10. Axial, out-of-plane, and shear stress contours for Case 2.

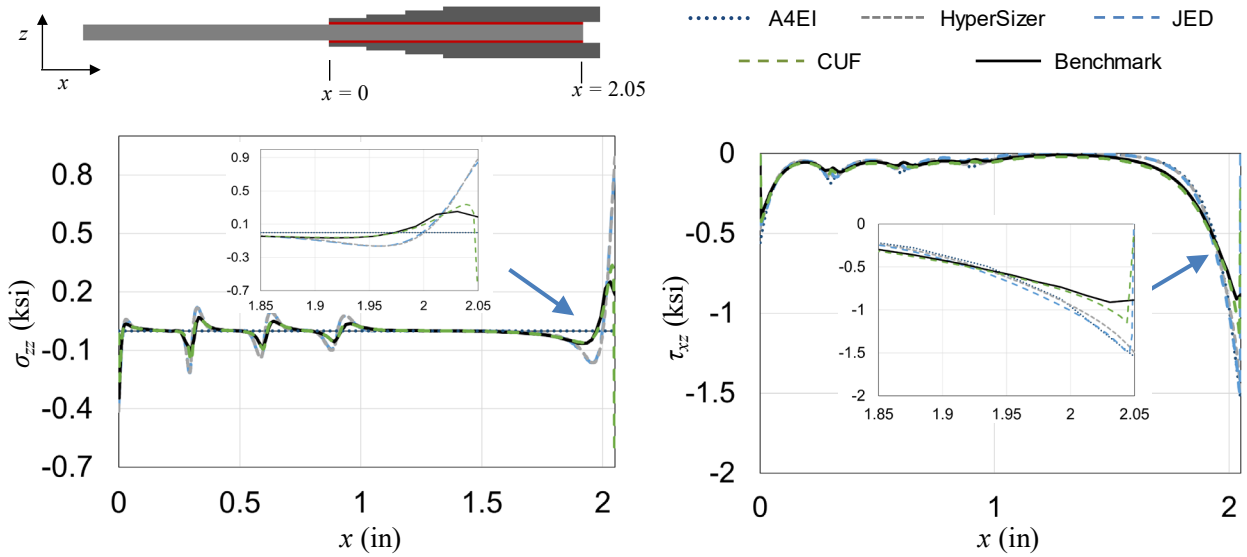

Figure 11. Peel (left) and shear (right) stresses along the top adhesive centerline of Case 3.

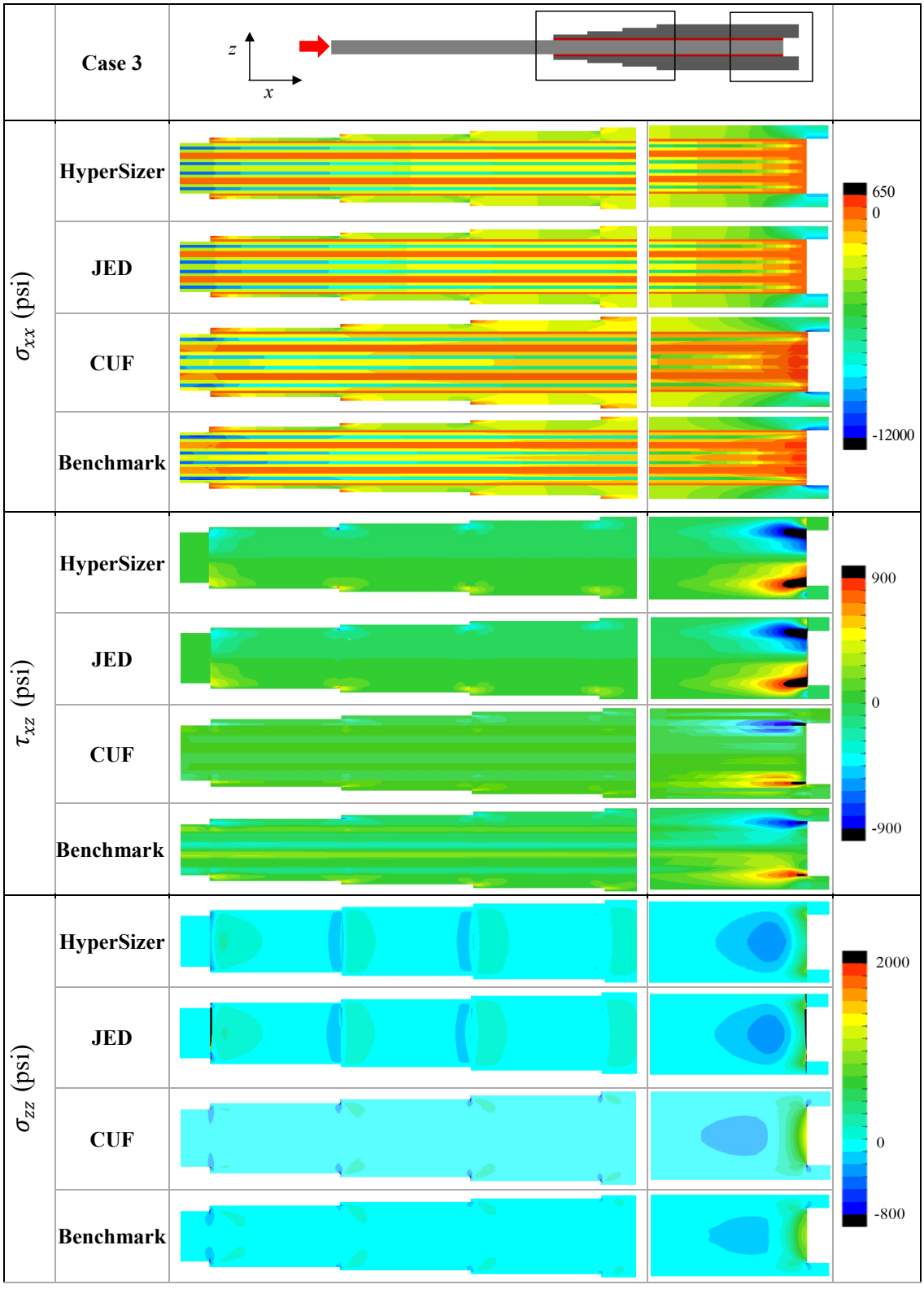

Figure 12. Axial, out-of-plane, and shear stress contours for Case 3.

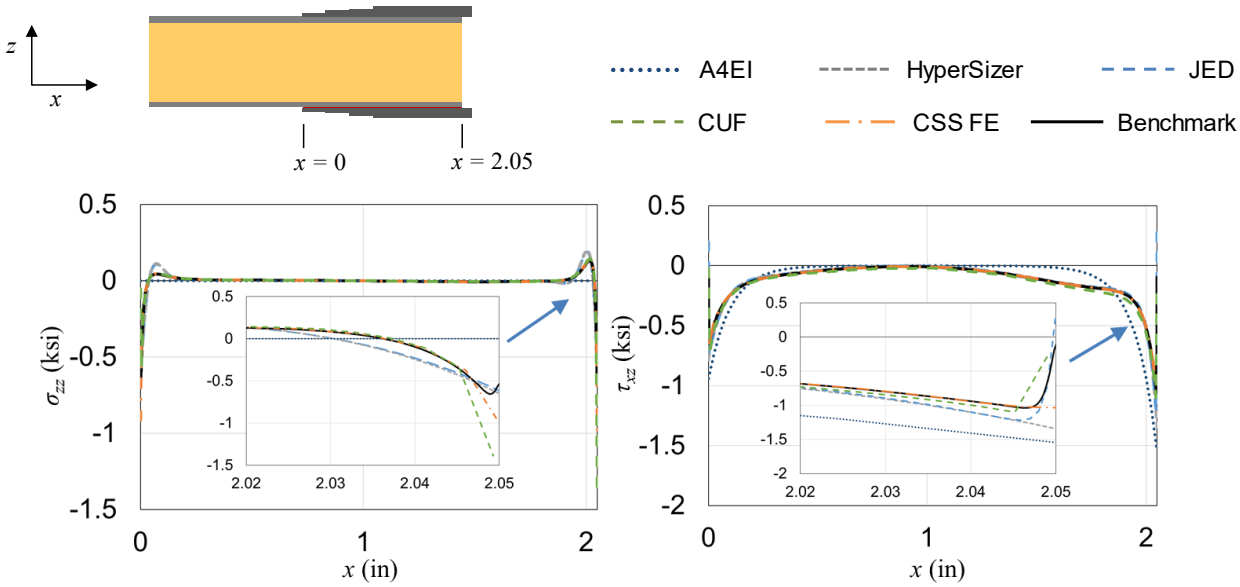

Figure 13. Peel (left) and shear (right) stresses along the top adhesive centerline of Case 4.

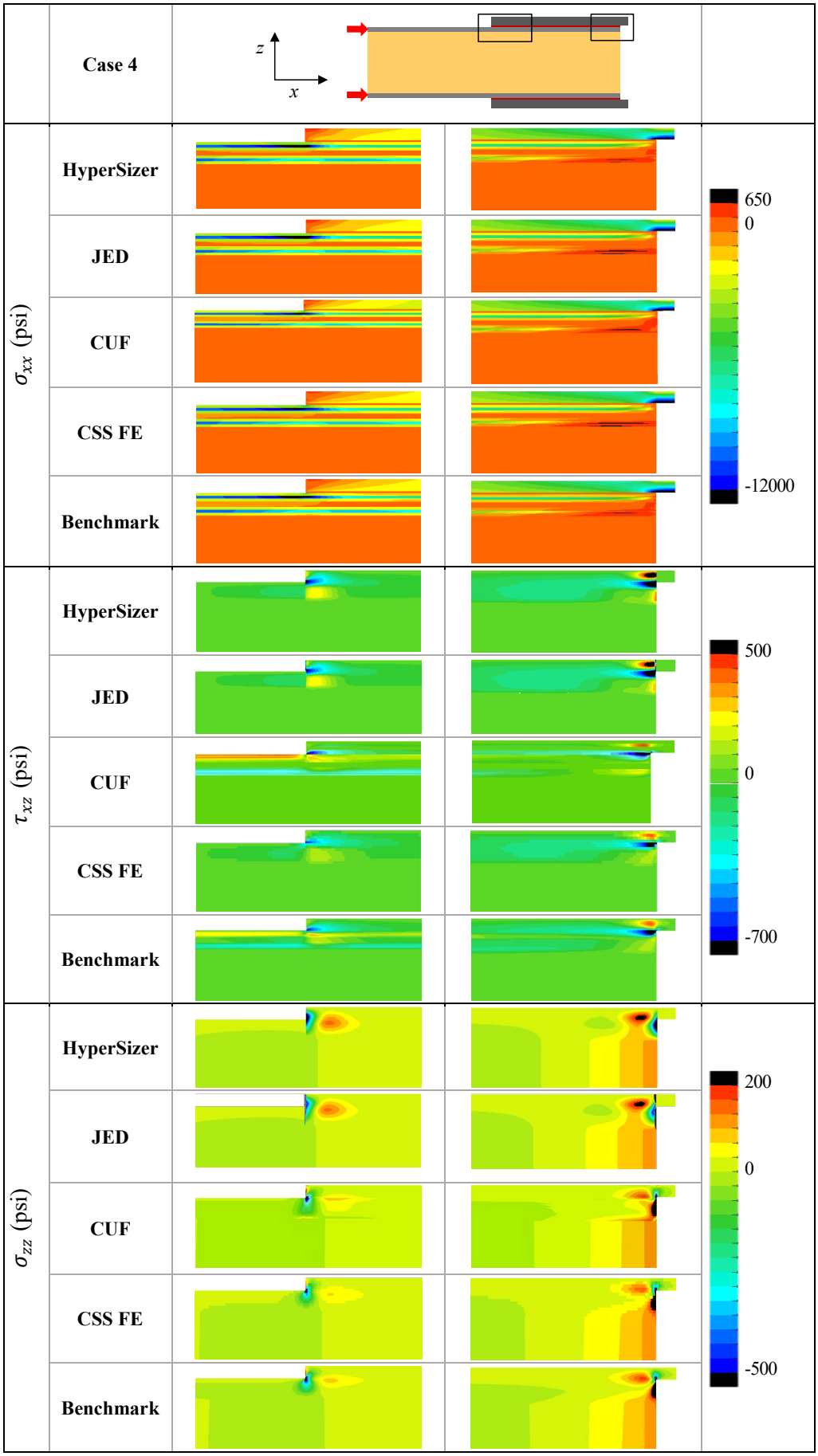

Figure 14. Axial, out-of-plane, and shear stress contours for Case 4.

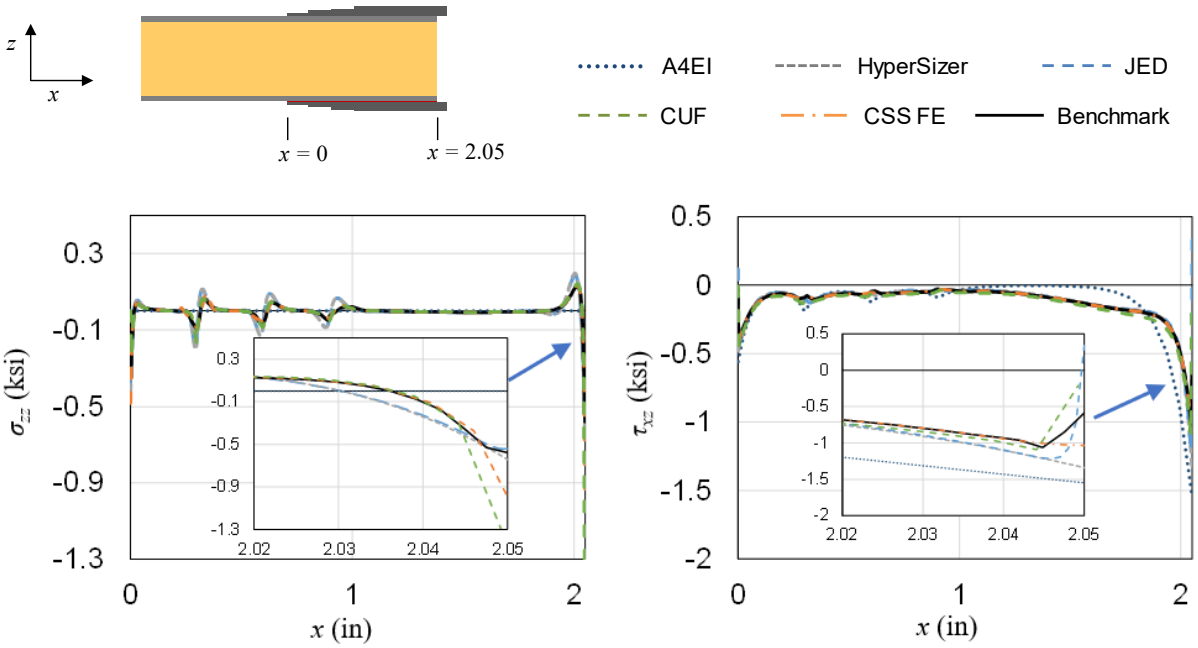

Figure 15. Peel (left) and shear (right) stresses along the top adhesive centerline of Case 5.

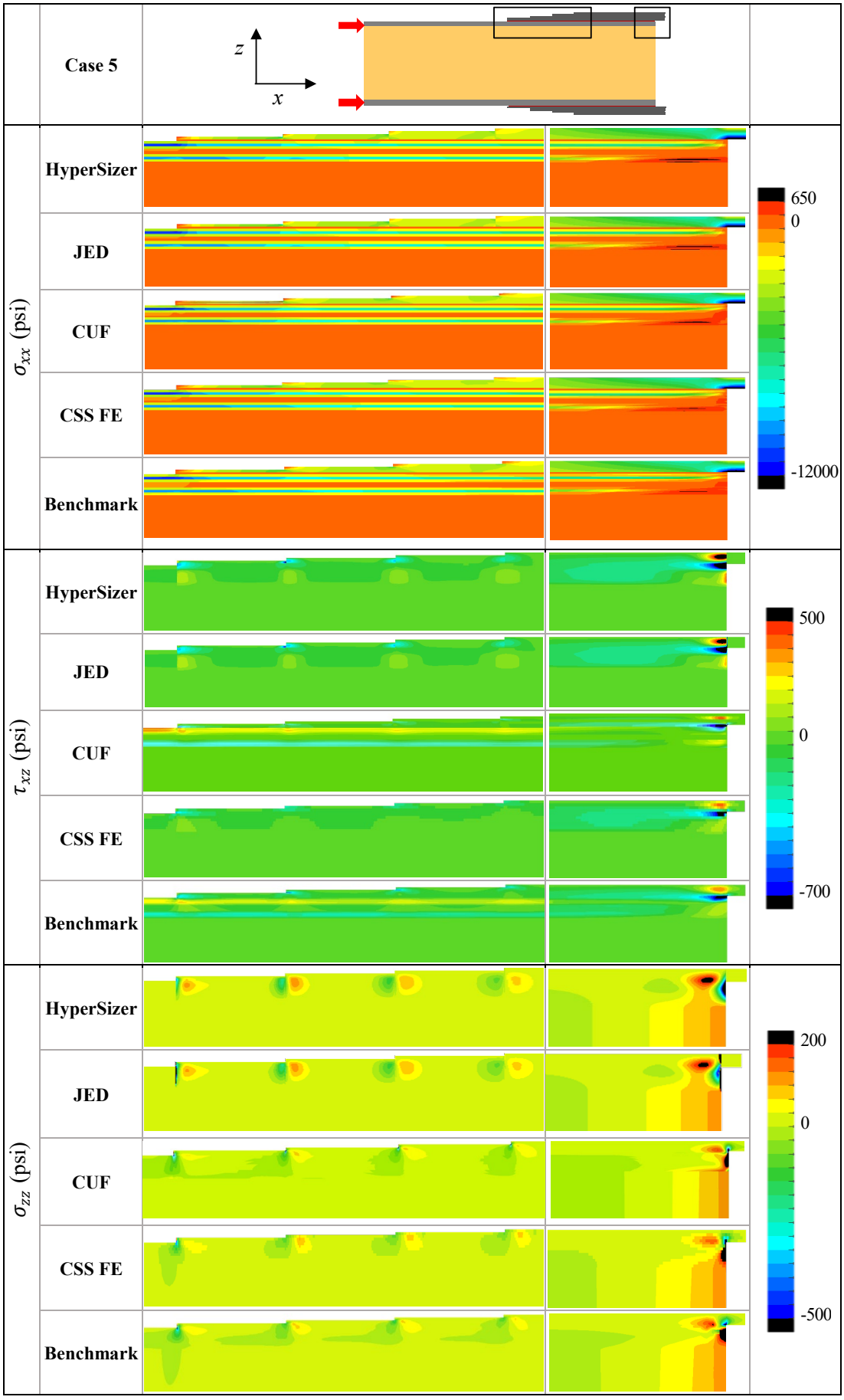

Figure 16. Axial, out-of-plane, and shear stress contours for Case 5.

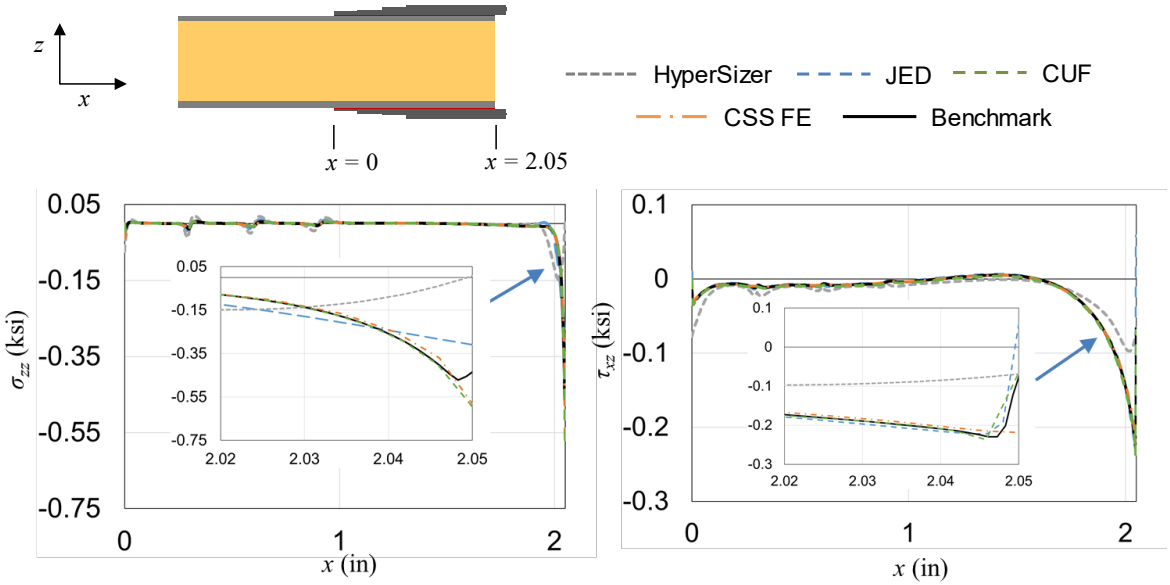

Figure 17. Peel (left) and shear (right) stresses along the top adhesive centerline of Case 6.

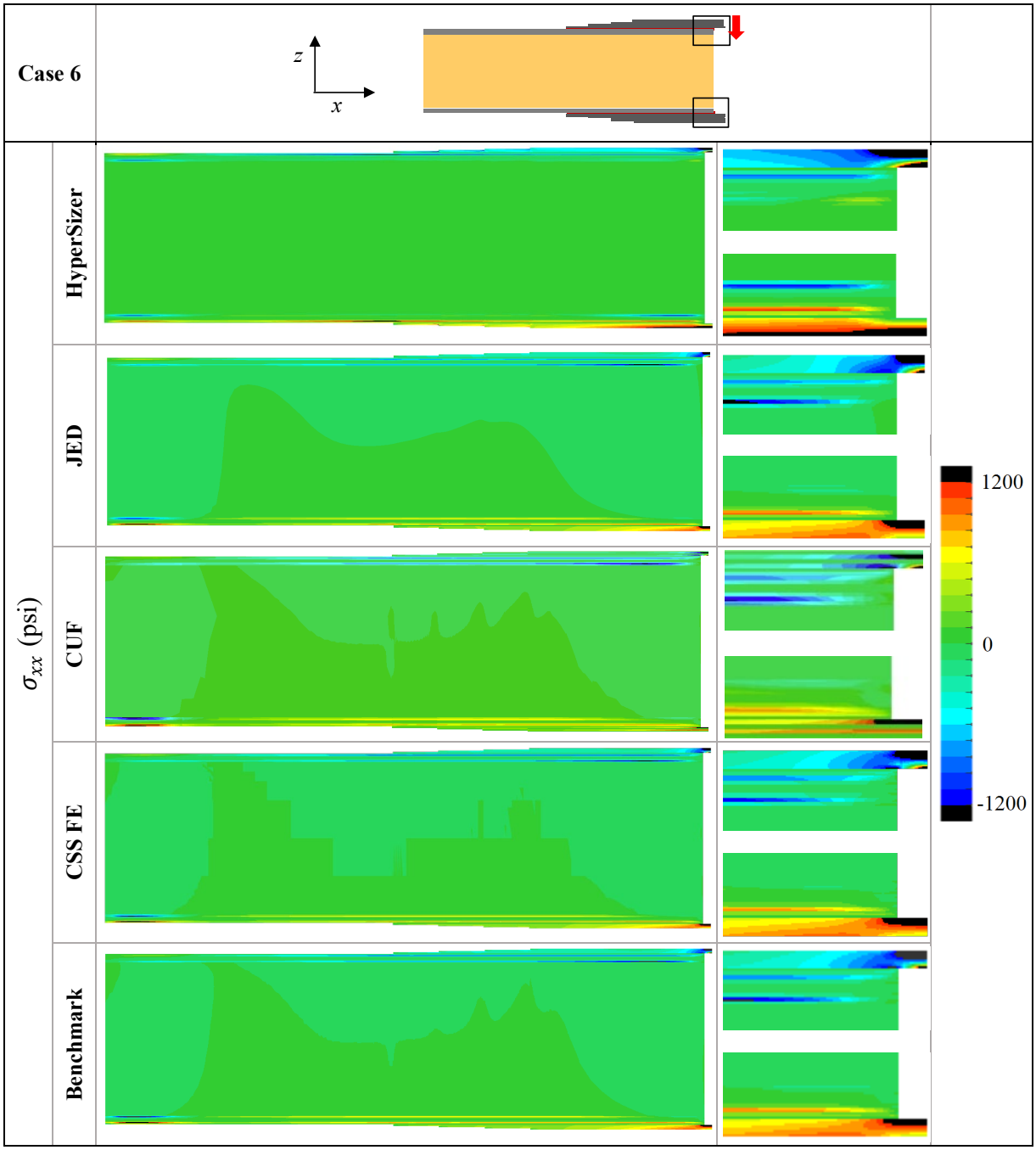

Figure 18. Axial stress contours for Case 6.

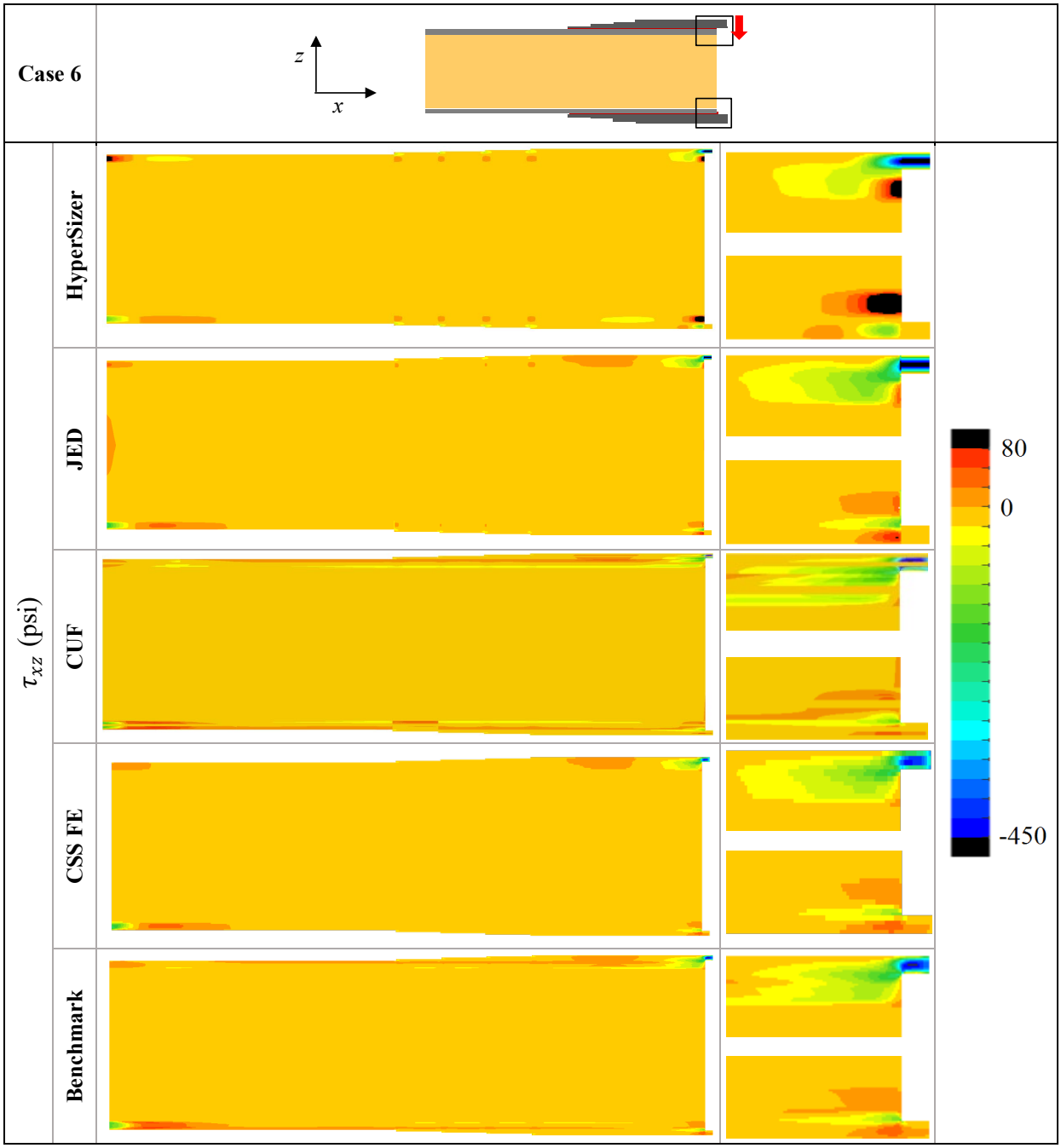

Figure 19. Shear stress contours for Case 6.

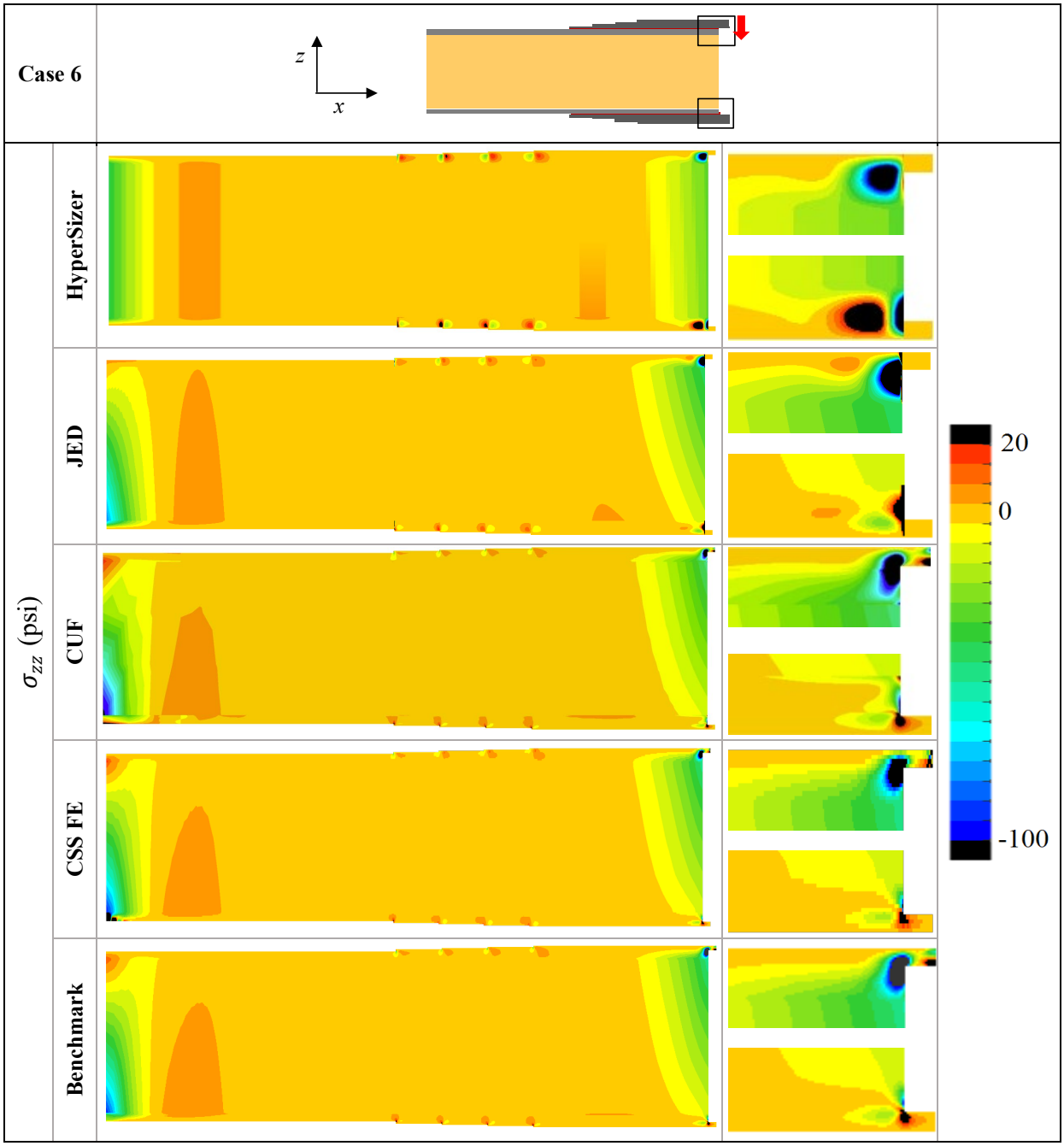

Figure 20. Out-of-plane stress contours for Case 6.

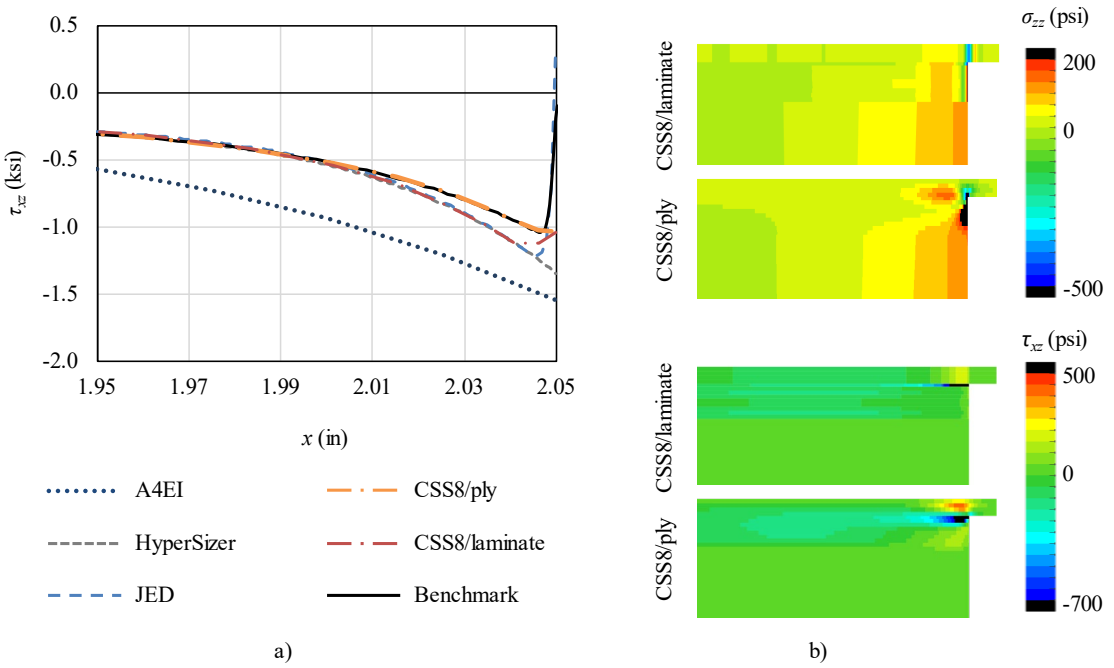

Figure 21. Effect of through the thickness mesh refinement on the CSS FE model stress fields for Case 4.